

# Chloroform–nitrogen aggregates: upshifted CH and downshifted CCl stretching vibrations observed by matrix isolation and jet expansion infrared spectroscopy

S. Oswald

*Institut für Physikalische Chemie, Universität Göttingen, Tammannstr. 6, 37077 Göttingen, Germany*

S. Coussan

*Aix-Marseille Université, CNRS, UMR 7345, Laboratoire Physique des Interactions Ioniques et Moléculaires, Marseille, France*

E-mail: stephane.coussan@univ-amu.fr

Received December 22, 2018, published online April 26, 2019

Aggregates of chloroform with nitrogen are studied by broad band Fourier transform infrared spectroscopy in neon, argon and nitrogen cryomatrices as well as supersonic jet expansions. The CH stretching vibration  $\nu_1$  shows spectral blue-shifting upon switching from isolated gas phase conditions to bulk nitrogen matrices, which can be reconstructed incrementally by stepwise cluster formation with an increasing amount of N<sub>2</sub> both in supersonic expansions and neon or argon matrices. Vice versa, the CCl stretching vibration  $\nu_5$  is incrementally downshifted. A small CH stretching upshift is observed in the chloroform homodimer as well.

Keywords: supersonic jet expansion, FTIR, aggregates, frequency shift.

## 1. Introduction

The formation of XH···Y hydrogen bonds is typically associated with an elongation of the XH bond and a corresponding spectral downshift of the XH stretching vibration [1–3]. However, some combinations of hydrogen bond donor and acceptor, often involving electron-deficient CH bonds [4–6], result in hydrogen bonding marked by spectral XH stretching blue-shifts [7–10]. Haloforms such as chloroform (CHCl<sub>3</sub>) offer the possibility of such blue-shifting hydrogen bonding [11] depending on the acceptor [12–14].

Chloroform itself and various aggregates have been extensively studied by infrared [13–18], microwave [19] and cavity ring-down [20] spectroscopy as well as vibrationally assisted dissociation and photofragment ionization [21] in the gas phase and infrared spectroscopy in liquid krypton [22] as well as cryogenic argon matrices [12,23], which found a smooth transition from up- to downshifts of the CH stretching vibration with varying hydrogen bond acceptors such as N<sub>2</sub>, CO, H<sub>2</sub>O, and CH<sub>3</sub>CN [12]. In supersonic expansion and gas phase, adducts of chloroform and ammonia show significant downshifts [14,24], while SO<sub>2</sub> complexation induces an upshift [13,25].

In the present contribution we confirm the CH stretching blue-shift in the hydrogen bonded chloroform nitrogen complex in neon and argon matrices, which is also repeated in the gas-to-matrix shift between isolated monomers in the gas phase and in bulk nitrogen matrices. The chloroform homodimer in helium expansions also displays a small CH stretching upshift. Signs of cluster formation are also observed in the very intense, doubly degenerate and *E*-symmetric CCl stretching mode, which is downshifted from the monomer band position.

## 2. Experimental section

Gas mixtures for matrix isolation experiments [26–29] were prepared with chloroform (Carlo Erba, 99.9%, stabilized with 0.6–1% ethanol) purified from solved gases through multiple freeze-pump-thaw cycles under primary vacuum. The partial ratio C/N<sub>2</sub>/MG (C, chloroform, MG, matrix gas) in the matrix gases neon (Air Liquide, N50 grade), argon and nitrogen (Air Liquide, N60 grade) ranged from 1.3/0/1000 to 5/150/1000. A gold-plated copper cube cooled to 4.7 K for neon and 20 K for argon and nitrogen matrices by a closed-cycle cryogenerator (Cryomech, PT-405) served as sample-carrier for deposition. A chrome-plated brass shield kept at  $\approx$  32 K protected both

cryogenic head and sample-carrier from thermal background radiation. A  $50\ \Omega$  resistor was used for controlled heating (Lakeshore, Model 336) of the sample carrier, while a turbomolecular pump ensured a background pressure of  $10^{-7}$  mbar in the vacuum chamber. Fourier transform infrared (FTIR) spectra were all recorded at 4.7 K in the reflection mode using a Bruker IFS 66/S spectrometer (resolution:  $0.12\ \text{cm}^{-1}$ ) equipped with a MCT detector.

Pulsed supersonic expansions [30] were performed with premixed gas compositions comprised of helium (Linde, 99.996%) and chloroform (TCI, > 99%, stabilized with ethanol) optionally mixed with nitrogen (Air Liquide, 99.999%) in partial ratios ( $\text{C}/\text{N}_2/\text{He}$ ) ranging from 1/25/1000 to 1/150/1000. The gas was stored in a 67 L Teflon coated reservoir at a stagnation pressure of 0.75 bar, guided into a preexpansion chamber via six high throughput solenoid valves and entered the vacuum chamber through a  $(600 \times 0.2)\ \text{mm}^2$  slit nozzle. The resulting supersonic expansion was probed perpendicularly by the infrared beam from a Bruker IFS 66v/S FTIR spectrometer at a resolution of  $2\ \text{cm}^{-1}$  equipped with a 150 W tungsten lamp,  $\text{CaF}_2$  optics and a liquid nitrogen cooled  $3\ \text{mm}^2$  InSb detector. Sufficiently low background pressures of 0.1 mbar during 147 ms gas pulses to minimize recompression shock waves caused by background gas were maintained by an attached  $23\ \text{m}^3$  buffer volume, a series of roots pumps at a speed of  $2500\ \text{m}^3 \cdot \text{h}^{-1}$  and a 25 s delay between subsequent pulses. A more detailed description of the setup (*filet-jet*) can be found in Ref. 30.

### 3. Quantum chemical calculations and nomenclature

Employed molecule abbreviations (C, chloroform, N, nitrogen) are repeated in hydrogen bond direction to describe cluster compositions according to the number of monomer units present in an aggregate. Possible docking sites of the acceptor molecule at chloroform include the CH proton (H) as well as the carbon (C) and one of the chlorine atoms (Cl), respectively, and are marked by subscripts at the hydrogen bond acceptor molecule. The most stable  $\text{C}_{\text{Cl}}\text{C}_{\text{Cl}}$  homodimer of chloroform (Fig. 1, see also higher energy conformers in Fig. S1, Supplementary material (SM)) features a double  $\text{CH}\cdots\text{Cl}$  hydrogen bond, differing from the minimum energy  $\text{CC}_\text{C}$  structure found at the MP2/aVQZ level [31].

The most stable heteroaggregates with nitrogen (Fig. 1, see also higher energy conformers in Figs. S2–S7, SM) display a progressive coordination of the CH group with increasing nitrogen addition, correlating with predicted spectral CH stretching upshifts and significant infrared intensity enhancements (Table 1, predictions for higher energy conformers in Table S2, SM). Predictions for the doubly degenerate CCl stretching vibration are somewhat ambiguous with small spectral upshifts for the first part and small downshifts for the second part (Table 2, predictions for higher energy conformers in Table S3, SM). Predicted dissociation

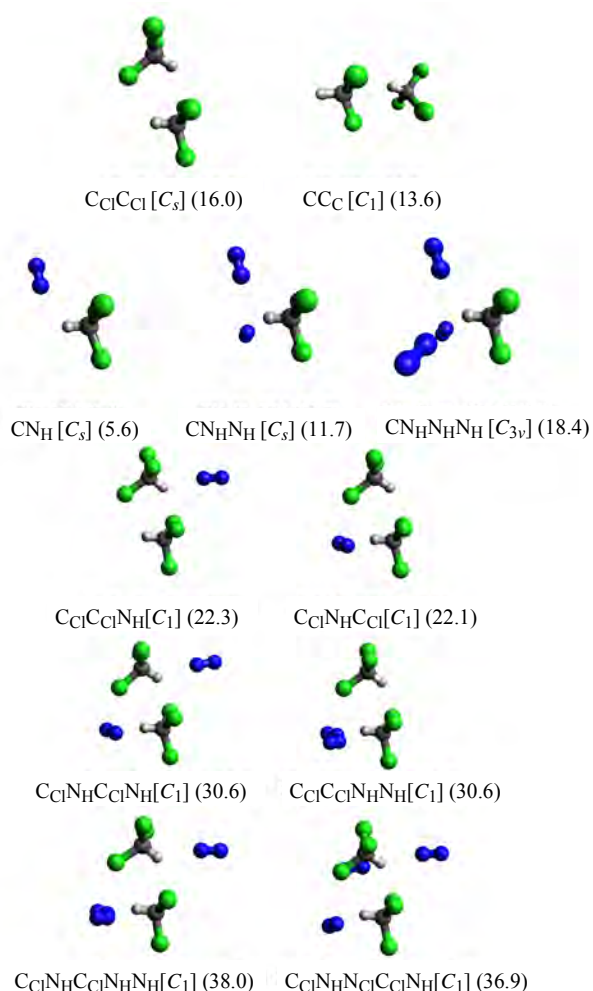


*Fig. 1.* Most stable structures of chloroform homo- and hetero-aggregates with nitrogen optimized at the B3LYP-D3(BJ)/def2-QZVP level. Molecular symmetry point groups are given in brackets, dissociation energies into stable monomers including harmonic vibrational zero-point correction in  $\text{kJ}\cdot\text{mol}^{-1}$  in parentheses.

energies for nitrogen complexation are about one third of the homodimer formation energy, therefore competition between both needs to be avoided by choosing appropriate experimental conditions such as low chloroform concentrations in both cryogenic matrices and supersonic jet expansions.

Anharmonic vibrational frequencies calculated with second order vibrational perturbation theory (Gaussian09 Rev. E01 [32], VPT2 [33]) are unreliable due to unphysical predictions for low-frequency large amplitude motions which affect localized high-frequency modes like the CH stretching vibration through their respective coupling constants.

### 4. Results and discussion

With the broadband FTIR spectrometer, data for both the CH and CCl stretching vibrations in cryogenic matrices were obtained simultaneously, while spectra in helium expansions are restricted to the CH stretching region.

Table 1. Theoretically predicted harmonic ( $\omega_{\text{CH}}$ ) CH stretching wavenumbers for the  $^{35}\text{Cl}$  and  $^{37}\text{Cl}$  isotopologues as well as their respective difference in  $\text{cm}^{-1}$ , IR intensity ( $S$ ) in  $\text{km}\cdot\text{mol}^{-1}$ , spectroscopic shifts ( $\Delta\omega_{\text{CH}}$ ) relative to the corresponding vibration in the pure  $^{35}\text{Cl}$  chloroform monomers or dimers in  $\text{cm}^{-1}$ , lowest predicted harmonic ( $\omega_L$ ) wavenumber in  $\text{cm}^{-1}$ , dissociation energy into the most stable monomers without ( $D_e$ ) and with ( $D_0$ ) harmonic vibrational zero-point energy in  $\text{kJ}\cdot\text{mol}^{-1}$ . All properties were calculated at the B3LYP-D3(BJ)/def2QZVP level of theory

Structure	$\omega_{\text{CH},^{35}\text{Cl}}$	$S_\omega$	$\omega_{\text{CH},^{37}\text{Cl}}$	$S_\omega$	$\Delta\omega_{\text{CH},^{35}\text{Cl}}$	$\omega_{\text{CH},^{35}\text{Cl}} - \omega_{\text{CH},^{37}\text{Cl}}$	$\omega_L$	$D_e$	$D_0$
C	3169	1	3169	1	—	0	258	—	—
$\text{CClC}_{\text{Cl}}$	3183	13	3183	13	14	0	2	17.6	16.0
	3174	5	3174	5	5	0			
$\text{CC}_\text{C}$	3185	13	3185	13	16	0	12	15.0	13.6
	3170	2	3170	2	1	0			
$\text{CN}_\text{H}$	3185	4	3185	4	16	0	21	7.2	5.6
$\text{CN}_\text{H}\text{N}_\text{H}$	3199	9	3199	9	30	0	11	14.8	11.7
$\text{CN}_\text{H}\text{N}_\text{H}\text{N}_\text{H}$	3216	17	3216	17	47	0	10	22.8	18.4
$\text{C}_{\text{Cl}}\text{C}_{\text{Cl}}\text{N}_\text{H}$	3201	19	3201	19	18	0	10	26.6	23.3
	3174	5	3174	5	0	0			
$\text{C}_{\text{Cl}}\text{N}_\text{H}\text{C}_{\text{Cl}}$	3189	9	3189	9	6	0	9	26.3	23.1
	3180	13	3180	13	6	0			
$\text{C}_{\text{Cl}}\text{N}_\text{H}\text{C}_{\text{Cl}}\text{N}_\text{H}$	3199	18	3199	18	16	0	9	35.4	30.6
	3189	10	3189	10	15	0			
$\text{C}_{\text{Cl}}\text{C}_{\text{Cl}}\text{N}_\text{H}\text{N}_\text{H}$	3206	16	3206	16	23	0	4	35.3	30.6
	3182	13	3182	13	8	0			
$\text{C}_{\text{Cl}}\text{N}_\text{H}\text{C}_{\text{Cl}}\text{N}_\text{H}\text{N}_\text{H}$	3206	17	3206	17	23	0	7	44.4	38.0
	3200	18	3200	18	26	0			
$\text{C}_{\text{Cl}}\text{N}_\text{H}\text{N}_{\text{Cl}}\text{C}_{\text{Cl}}\text{N}_\text{H}$	3198	18	3198	18	15	0	11	43.1	36.9
	3189	10	3189	10	15	0			

#### 4.1. Neon, argon and nitrogen matrices

##### 4.1.1. CH stretching vibration $v_1$

Highly diluted mixtures of chloroform in different matrix hosts were deposited to minimize the formation of homo-aggregates directly after deposition, which is energetically favoured over heterocomplex formation with nitrogen. The CH stretching signal in neon matrix (Fig. 2) observed at  $3039.8\text{ cm}^{-1}$  is weak in accordance with the calculated low infrared band strength. The band gains intensity after annealing and broadens to higher wavenumbers, indicating the formation of chloroform homoclusters with upshifted CH stretching vibrations and higher infrared band strengths. Another band emerging upon annealing at  $3017.5\text{ cm}^{-1}$  is possibly due to the second CH stretching mode of the most stable dimer ( $\text{C}_{\text{Cl}}\text{C}_{\text{Cl}}$ ), or caused by a second chloroform dimer conformation ( $\text{CC}_\text{C}$  or  $\text{CC}_{\text{Cl}}$ ) or the trimer. The reversed direction of the wavenumber shift has previously been observed for CH stretching modes and the contradiction of the uniform upshift predictions for chloroform dimers underscores the difficulties in theoretical modelling of this weak perturbation [34].

The monomer band centre in argon matrix is found at  $3054.1\text{ cm}^{-1}$  (Fig. 3), in reasonable agreement with a previous study by Ito ( $3053\text{ cm}^{-1}$ ) [12] at slightly lower resolution. After annealing to 39 K two small features down-

shifted to  $3052.1$  and  $3038.9\text{ cm}^{-1}$  emerge, likely caused by the chloroform dimer. Hence, the direction of the CH stretching shift induced by chloroform homocluster formation is partly reversed in argon matrices when compared to neon hosts.

In nitrogen matrix (Fig. 4) the chloroform monomer shows significant site splitting with a dominant band at  $3066.6\text{ cm}^{-1}$  and two weak signals at  $3053.4$  and  $3039.2\text{ cm}^{-1}$ , respectively. Both unstable sites are depopulated upon annealing and one of the two dimer vibrations emerges at  $3030.0\text{ cm}^{-1}$ , downshifted from the monomer as observed in the case of argon matrices. The dominant monomer site at  $3066.6\text{ cm}^{-1}$  and the high resolution gas phase band centre position [13,35] of  $3032.92642(25)\text{ cm}^{-1}$  allow for an accurate determination of the total gas-to-nitrogen-matrix shift, which amounts to  $33.7\text{ cm}^{-1}$ , significantly larger than the gas-to-argon matrix shift of  $21.1\text{ cm}^{-1}$  and the gas-to-neon matrix shift of  $6.9\text{ cm}^{-1}$ .

##### 4.1.2. CCl stretching vibration $v_5$

In neon matrices, a small shoulder at  $765.3\text{ cm}^{-1}$  assigned to the chloroform dimer grows in after annealing, downshifted from the broad and highly structured monomer CCl stretching signal with multiple peaks between  $776.4$  and  $768.4\text{ cm}^{-1}$  (Fig. 5). Part of this structure and width can be attributed to the different isotopomers with

Table 2. Theoretically predicted harmonic ( $\omega_{\text{CCl}}$ ) CCl stretching wavenumbers for the  $^{35}\text{Cl}$  and  $^{37}\text{Cl}$  isotopologues as well as their respective difference in  $\text{cm}^{-1}$ , IR intensity ( $S$ ) in  $\text{km}\cdot\text{mol}^{-1}$ , spectroscopic shifts ( $\Delta\omega_{\text{CH}}$ ) relative to the corresponding vibration in the pure  $^{35}\text{Cl}$  chloroform monomers or dimers in  $\text{cm}^{-1}$ , lowest predicted harmonic ( $\omega_L$ ) wavenumber in  $\text{cm}^{-1}$ , dissociation energy into the most stable monomers without ( $D_e$ ) and with ( $D_0$ ) harmonic vibrational zero-point energy in  $\text{kJ}\cdot\text{mol}^{-1}$ . All properties were calculated at the B3LYP-D3(BJ)/def2QZVP level of theory

Structure	$\omega_{\text{C},^{35}\text{Cl}}$	$S_\omega$	$\omega_{\text{C},^{37}\text{Cl}}$	$S_\omega$	$\Delta\omega_{\text{C},^{35}\text{Cl}}$	$\omega_{\text{C},^{35}\text{Cl}} - \omega_{\text{C},^{37}\text{Cl}}$	$\omega_L$	$D_e$	$D_0$
C	733	161	730	160	—	3	258	—	—
	733	161	730	160	—	3			
$\text{C}_{\text{Cl}}\text{C}_{\text{Cl}}$	744	228	740	226	11	4	2	17.6	16.0
	742	123	739	121	9	3			
	725	220	722	219	-8	3			
	723	38	719	37	-10	4			
$\text{CC}_\text{C}$	740	260	737	257	7	3	12	15.0	13.6
	737	261	733	259	4	4			
	734	28	730	27	1	4			
	722	16	719	16	-11	3			
$\text{CN}_\text{H}$	736	169	733	168	3	3	21	7.2	5.6
	732	153	728	152	-1	4			
$\text{CN}_\text{H}\text{N}_\text{H}$	737	167	733	165	4	4	11	14.8	11.7
	732	155	729	153	-1	3			
$\text{CN}_\text{H}\text{N}_\text{H}\text{N}_\text{H}$	735	160	732	158	2	3	10	22.8	18.4
	735	160	732	158	2	3			
$\text{C}_{\text{Cl}}\text{C}_{\text{Cl}}\text{N}_\text{H}$	744	193	740	190	0	4	10	26.6	23.3
	741	151	738	149	-1	3			
	727	208	723	208	2	4			
	723	53	719	52	0	4			
$\text{C}_{\text{Cl}}\text{N}_\text{H}\text{C}_{\text{Cl}}$	744	207	740	205	0	4	9	26.3	23.1
	742	142	739	140	0	3			
	726	205	723	204	1	3			
	723	54	719	54	0	4			
$\text{C}_{\text{Cl}}\text{N}_\text{H}\text{C}_{\text{Cl}}\text{N}_\text{H}$	743	180	740	177	-1	3	9	35.4	30.6
	741	160	738	157	-1	3			
	727	215	724	215	2	3			
	723	51	720	49	0	3			
$\text{C}_{\text{Cl}}\text{C}_{\text{Cl}}\text{N}_\text{H}\text{N}_\text{H}$	744	222	740	220	0	4	4	35.3	30.6
	742	127	739	125	0	3			
	726	211	723	209	1	3			
	724	51	720	51	1	4			
$\text{C}_{\text{Cl}}\text{N}_\text{H}\text{C}_{\text{Cl}}\text{N}_\text{H}\text{N}_\text{H}$	744	191	740	189	0	4	7	44.4	38.0
	741	149	738	147	-1	3			
	728	210	725	209	3	3			
	724	57	720	56	1	4			
$\text{C}_{\text{Cl}}\text{N}_\text{H}\text{N}_\text{Cl}\text{C}_{\text{Cl}}\text{N}_\text{H}$	744	186	741	183	0	3	11	43.1	36.9
	740	176	736	174	-2	4			
	728	161	725	162	3	3			
	723	84	720	82	0	3			

various combinations of  $^{35}\text{Cl}$  and  $^{37}\text{Cl}$ . While the CH stretching mode is unaffected by the isotope substitution (Table 1), CCl stretching wavenumbers are lowered by about  $3\text{--}4\text{ cm}^{-1}$  (Table 2) when changing all chlorine atoms to the heavier  $^{37}\text{Cl}$  isotope. In addition, interactions with

the matrix host might lift the degeneracy of the vibrational  $E$ -symmetric levels.

A similarly broad and structured signal ranging from  $769.9$  to  $763.7\text{ cm}^{-1}$  is found in argon matrix (Fig. 6) and

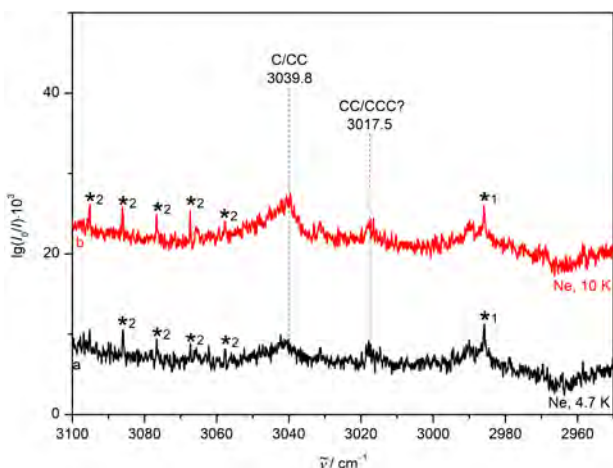


Fig. 2. CH stretching FTIR spectra of 0.13% chloroform in neon matrix after deposition at 4.7 K (trace a) and after annealing to 10 K and recooling to 4.7 K (trace b). Wavenumbers and (tentative) assignments are provided. Vibrational signals assigned to the ethanol stabilizer (\*1) and methane (\*2) are marked by asterisks.

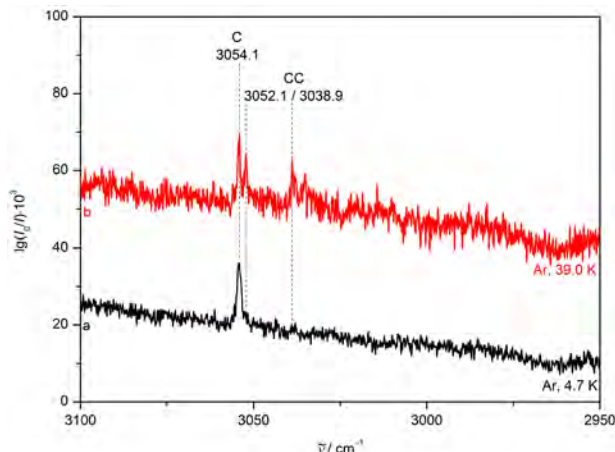


Fig. 3. CH stretching FTIR spectra of 0.13% chloroform in argon matrix after deposition at 20 K and subsequent cooling to 4.7 K (trace a) and after annealing to 39 K and recooling to 4.7 K (trace b). Wavenumbers and (tentative) assignments are provided.

various dimer vibrations emerge with a slight downshift between 761.9 and 756.0  $\text{cm}^{-1}$  after annealing.

The signal in nitrogen matrix (Fig. 7) ranges from 770.2 to 761.6  $\text{cm}^{-1}$ . Several peaks at 768.4, 767.1 and 764.6  $\text{cm}^{-1}$  gain intensity relative to the remaining signals after annealing, which could be a sign of unstable site depopulation or dimer formation.

The intensity ratio of the CH and CCl stretching modes changes significantly with the different matrix hosts. While the CCl stretching band strength appears to be relatively independent of the matrix host (Table 2), the CH stretching intensity increases from weakly interacting neon over more polarizable argon to quadrupolar nitrogen, resulting in an approximate three-fold enhancement of the ratio  $S_{\text{CH}}/S_{\text{CCl}}$  when comparing neon and nitrogen matrices (Fig. 8). This

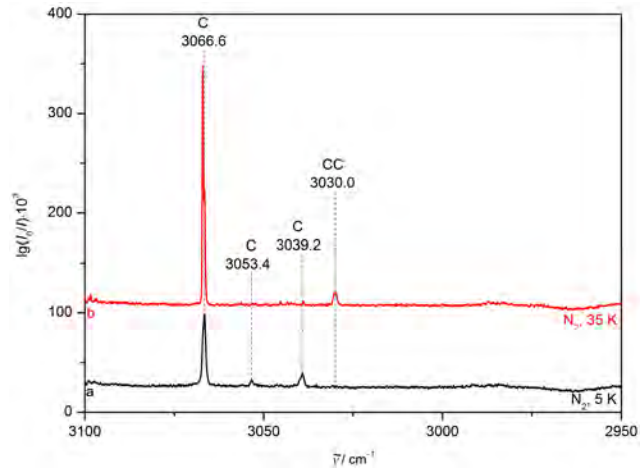


Fig. 4. CH stretching FTIR spectra of 0.13% chloroform in nitrogen matrix after deposition at 20 K and subsequent cooling to 5 K (trace a) and after annealing to 35 K and recooling to 5 K (trace b). Wavenumbers and (tentative) assignments are provided.

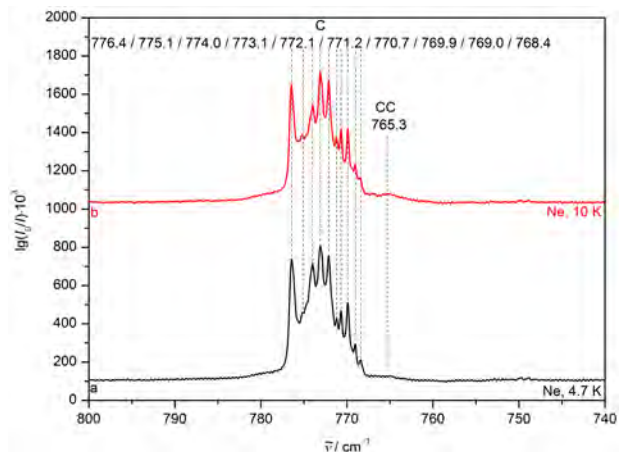


Fig. 5. CCl stretching FTIR spectra of 0.13% chloroform in neon matrix after deposition at 4.7 K (trace a) and after annealing to 10 K and recooling to 4.7 K (trace b). Wavenumbers and (tentative) assignments are provided.

behavior is also found for other modes sensitive to intermolecular interaction such as OH [36,37] or NH [38] stretching vibrations.

#### 4.2. Nitrogen added to neon and argon matrices

##### 4.2.1. CH stretching vibration $v_1$

Stepwise addition of nitrogen to neon matrices (Fig. 9) induces broad CH stretching signals which are incrementally upshifted from the original peak at 3039.8  $\text{cm}^{-1}$  and approach the position of the dominant site in nitrogen matrix at 3066.6  $\text{cm}^{-1}$ , while upshift and signal intensity increase upon annealing. The broad signal is indicative of an incomplete and amorphous chloroform embedding in nitrogen enriched neon matrix grains, which leads to an inho-

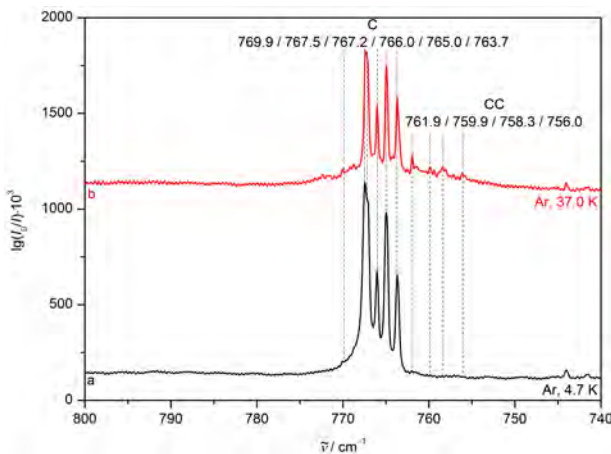


Fig. 6. CCl stretching FTIR spectra of 0.13% chloroform in argon matrix after deposition at 20 K and subsequent cooling to 4.7 K (trace a) and after annealing to 37 K and recooling to 4.7 K (trace b). Wavenumbers and (tentative) assignments are provided.

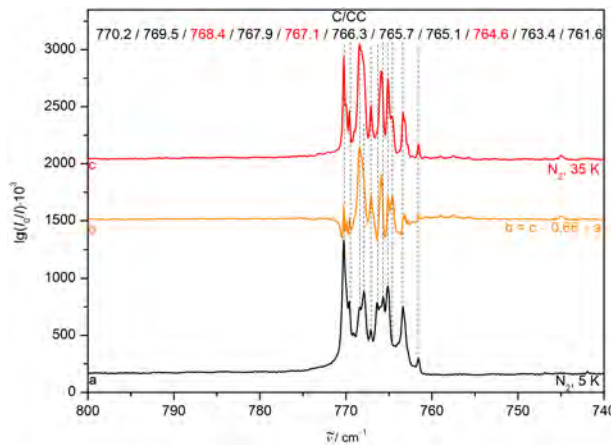


Fig. 7. CCl stretching FTIR spectra of 0.13% chloroform in nitrogen matrix after deposition at 20 K and subsequent cooling to 5 K (trace a) and after annealing to 35 K and recooling to 5 K (trace c). A difference spectrum is included (trace b). Wavenumbers and (tentative) assignments are provided. Vibrational bands which gain relative intensity after annealing are marked in red font.

mogeneous broadening induced by a more dispersed distribution of nearly equivalent oscillator classes. The distance of separated chloroform and nitrogen components in the neon matrix needs to be low enough to allow for formation of the aggregates through migration upon annealing.

Similar behavior is found in argon matrix (Fig. 10). The upshifted band position observed after nitrogen addition and annealing is in reasonable agreement with the  $11 \text{ cm}^{-1}$  upshift previously found by Ito [12] for the chloroform–nitrogen complex in argon matrix.

#### 4.2.2. CCl stretching vibration $\nu_5$

Very similar to the CH stretching vibration, the CCl stretching band is incrementally shifted towards the pure nitrogen matrix value after stepwise nitrogen addition

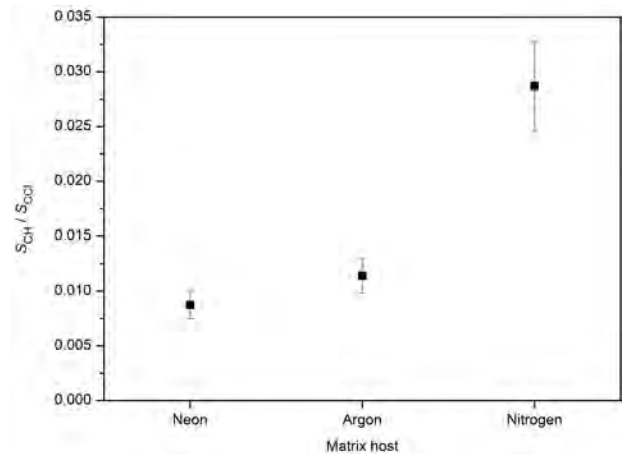


Fig. 8. Ratio of experimental CH ( $S_{\text{CH}}$ ) and CCl ( $S_{\text{CCl}}$ ) band integrals depending on the matrix host. Relative integral errors of 1% (CCl) and 10% (CH), respectively, were estimated based on the signal-to-noise ratio. While  $S_{\text{CCl}}$  is relatively independent of the matrix host,  $S_{\text{CH}}$  increases significantly from neon over argon to the strongly interacting nitrogen.

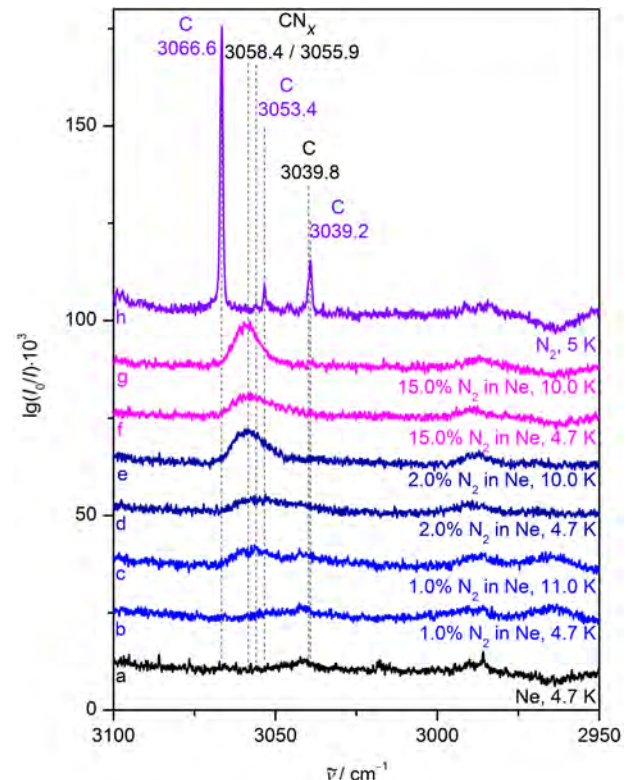


Fig. 9. CH stretching FTIR spectra of 0.13% chloroform in neon matrix after deposition at 4.7 K (trace a). Spectra of neon matrices with increasing nitrogen addition (traces b to g) before and after annealing to the stated temperature and subsequent recooling to 5 K as well as a nitrogen matrix deposited at 20 K and subsequently cooled to 4.7 K (trace h) are also included. Wavenumbers and (tentative) assignments are provided.

(Fig. 11), even more pronounced after annealing. However, the direction of the shift is reversed compared to the CH stretching and for the CCl stretching a small downshift is observed.

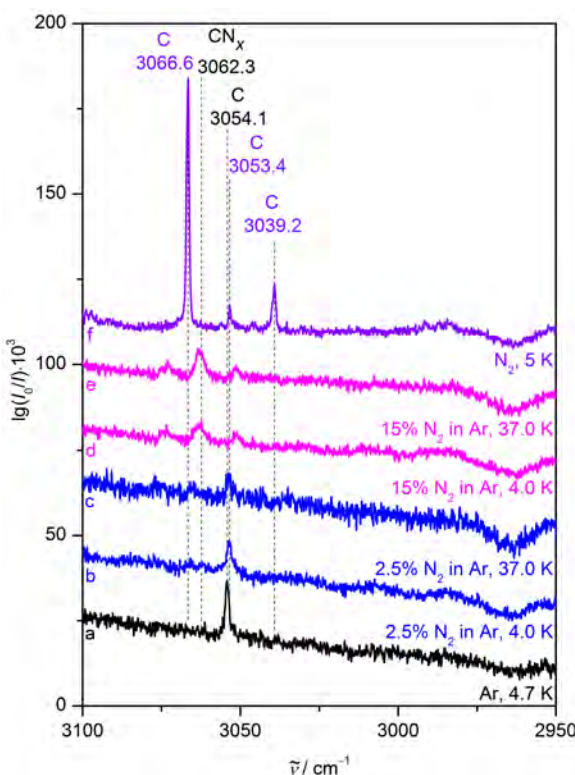


Fig. 10. CH stretching FTIR spectra of 0.13% chloroform in argon matrix after deposition at 20 K and subsequent cooling to 4.7 K (trace a). Spectra of argon matrices with increasing nitrogen addition (traces b to e) before and after annealing to the stated temperature and subsequent recooling to 4.7 K as well as a nitrogen matrix deposited at 20 K and subsequently cooled to 5 K (trace f) are also included. Wavenumbers and (tentative) assignments are provided.

The band positions in nitrogen and argon matrices are very similar (Fig. 12). Therefore, nitrogen addition to an argon matrix causes broadening of the band due to unspecific chloroform–nitrogen interactions, but no significant spectral shifts.

#### 4.3. Supersonic expansion

Moving from matrix isolation to supersonic helium expansions (Fig. 13) allows the determination of the chloroform monomer CH stretching band centre at 3033 cm<sup>-1</sup> without environmental influences by various matrix hosts, in agreement with the high resolution gas phase value [13,35] of 3032.92642(25) cm<sup>-1</sup>. Increasing the chloroform fraction in the expansion leads to a growing signal at 3037 cm<sup>-1</sup> caused by the chloroform dimer. This confirms previous unpublished work at higher resolution [39]. According to the cluster calculations (Table 1), a second dimer signal with a lower upshift and intensity enhancement is expected which is likely not observed due to spectral overlap with the monomer and the first dimer signal at the limited resolution of 2 cm<sup>-1</sup>.

Adding 15% N<sub>2</sub> to the carrier gas (Fig. 14) results in two new signals at 3043 and 3051 cm<sup>-1</sup>, respectively. Both

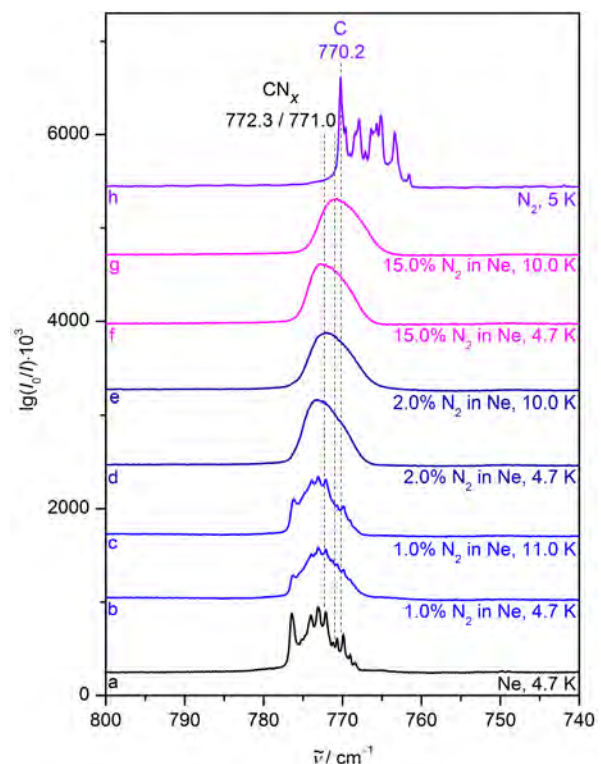


Fig. 11. CCl stretching FTIR spectra of 0.13% chloroform in neon matrix after deposition at 4.7 K (trace a). Spectra of neon matrices with increasing nitrogen addition (traces b to g) before and after annealing to the stated temperature and subsequent recooling to 4.7 K as well as a nitrogen matrix deposited at 20 K and subsequently cooled to 5 K (trace h) are also included. Wavenumbers and (tentative) assignments are provided.

are upshifted from the monomer band centre and can be assigned to various chloroform nitrogen clusters or even chloroform nanosolvated in nitrogen. The peak position shifts towards the dominant bulk matrix value with increasing nitrogen coordination without fully reaching it. The experimentally observed upshifts of 10 and 18 cm<sup>-1</sup> are in good agreement with harmonic predictions for CN<sub>H</sub> aggregates (Table 1).

#### 5. Conclusions

The CH stretching mode of chloroform exhibits an upshift of 33.7 cm<sup>-1</sup> when switching from isolated gas phase conditions to bulk nitrogen matrices. Incremental nitrogen complexation in neon and argon cryogenic matrices as well as supersonic helium expansions partially reproduces this effect (Fig. 15). Wavenumbers for small chloroform nitrogen clusters predicted by density functional theory calculations within the double harmonic approximation are able to describe this spectral evolution qualitatively, although the shift is overestimated for triple nitrogen coordination, which could be attributed to an electronic structure deficiency or neglected anharmonicity. Nitrogen cluster formation is also corroborated by downshifts of the intense CCl stretching

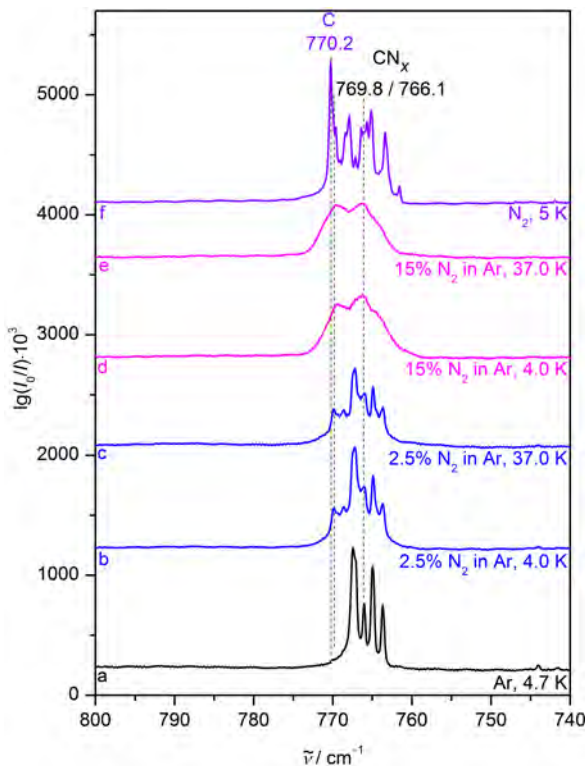


Fig. 12. CCl stretching FTIR spectra of 0.13% chloroform in argon matrix after deposition at 20 K and subsequent cooling to 4.7 K (trace a). Spectra of argon matrices with increasing nitrogen addition (traces b to e) before and after annealing to the stated temperature and subsequent recooling to 4.7 K as well as a nitrogen matrix deposited at 20 K and subsequently cooled to 5 K (trace f) are also included. Wavenumbers and (tentative) assignments are provided.

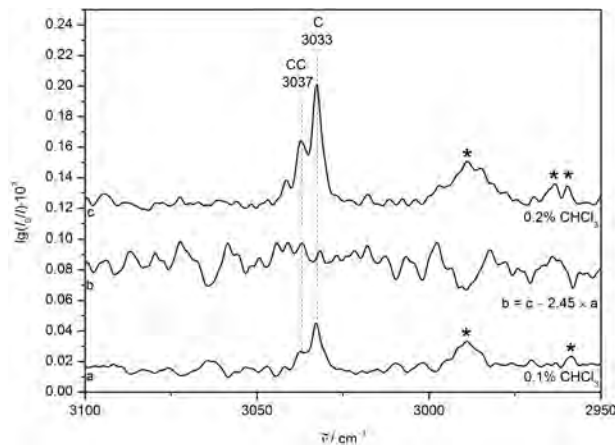


Fig. 13. FTIR jet spectra of chloroform expanded in helium as well as a monomer-corrected difference spectrum. Wavenumbers and (tentative) assignments are provided. Vibrational signals assigned to the ethanol stabilizer are marked by asterisks.

mode, while theoretical predictions for the doubly degenerate *E*-symmetric vibration are somewhat ambiguous.

Chloroform homodimers are observed as well both in matrices and jet expansions. Theoretically predicted shifts

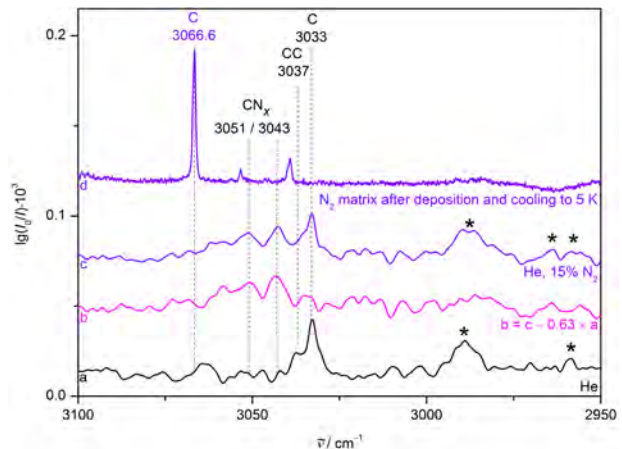


Fig. 14. FTIR jet spectra of chloroform expanded in helium (trace a) and a mixture of N<sub>2</sub> and helium (trace c) as well as a monomer-corrected difference spectrum (trace b). Wavenumbers, (tentative) assignments and a bulk nitrogen matrix spectrum (trace d) are provided. Vibrational signals assigned to the ethanol stabilizer are marked by asterisks.

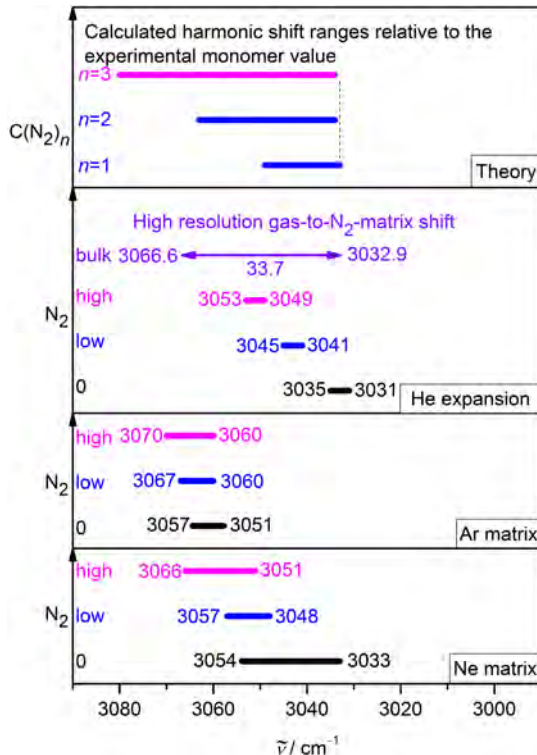


Fig. 15. CH stretching band positions of the chloroform monomer in neon and argon cryomatrices as well as in supersonic helium expansions. Increasing nitrogen admixture causes progressive upshifts of the band position in all three environments, approaching the bulk N<sub>2</sub> matrix limit. High resolution gas phase [13,35] and nitrogen matrix spectra allow for an accurate determination of the total gas-to-matrix upshift to 33.7 cm<sup>-1</sup>. The range of wavenumber shifts predicted for chloroform–nitrogen complexes by harmonic B3LYP-D3(BJ)/def2-QZVP calculations reproduces experimental findings with reasonable accuracy for the first two added nitrogen molecules, but the tested approach overestimates the upshift in more nitrogen-enriched environments, overshooting the bulk limit.

for these aggregates are somewhat unreliable, sometimes over- or underestimating the amount of the shift and even predicting the wrong sign in certain cases. The failure to accurately capture the weak observed effects is possibly partly due to electronic structure or anharmonicity deficiencies and partly caused by the finite size of calculated clusters failing to account for the bulk environment.

### Supplementary material

See [supplementary material](#) for higher energy conformers.

### Acknowledgments

We thank Martin A. Suhm for valuable and helpful discussions and access to the jet set-up. S. Oswald thanks the Fonds der Chemischen Industrie for a generous scholarship. We thank the Gesellschaft für wissenschaftliche Datenverarbeitung mbH Göttingen (GWDG) for access to their computing facilities.

1. A.V. Iogansen, *Spectrochim. Acta A* **55**, 1585 (1999).
2. E. Arunan, G.R. Desiraju, R.A. Klein, J. Sadlej, S. Scheiner, I. Alkorta, D.C. Clary, R.H. Crabtree, J.J. Dannenberg, P. Hobza, H.G. Kjaergaard, A.C. Legon, B. Mennucci, and D.J. Nesbitt, *Pure Appl. Chem.* **83**, 1619 (2011).
3. E. Arunan, G.R. Desiraju, R.A. Klein, J. Sadlej, S. Scheiner, I. Alkorta, D.C. Clary, R.H. Crabtree, J.J. Dannenberg, P. Hobza, H.G. Kjaergaard, A.C. Legon, B. Mennucci, and D.J. Nesbitt, *Pure Appl. Chem.* **83**, 1637 (2011).
4. H. Matsuura, H. Yoshida, M. Hieda, S.-y. Yamanaka, T. Harada, K. Shinya, and K. Ohno, *J. Am. Chem. Soc.* **125**, 13910 (2003).
5. A. Kovács, A. Szabó, D. Nemcsok, and I. Hargittai, *J. Phys. Chem. A* **106**, 5671 (2002).
6. P. Hobza, V. Špirko, Z. Havlas, K. Buchhold, B. Reimann, H.-D. Barth, and B. Brutschy, *Chem. Phys. Lett.* **299**, 180 (1999).
7. P. Hobza and Z. Havlas, *Chem. Rev.* **100**, 4253 (2000).
8. X. Li, L. Liu, and H.B. Schlegel, *J. Am. Chem. Soc.* **124**, 9639 (2002).
9. I.V. Alabugin, M. Manoharan, S. Peabody, and F. Weinhold, *J. Am. Chem. Soc.* **125**, 5973 (2003).
10. J. Joseph and E.D. Jemmis, *J. Am. Chem. Soc.* **129**, 4620 (2007).
11. A.J. Barnes, *J. Mol. Struct.* **100**, 259 (1983).
12. F. Ito, *J. Chem. Phys.* **137**, 014505 (2012).
13. S. Chung and M. Hippler, *J. Chem. Phys.* **124**, 214316 (2006).
14. M. Hippler, S. Hesse, and M.A. Suhm, *Phys. Chem. Chem. Phys.* **12**, 13555 (2010).
15. T.G. Gibian and D.S. McKinney, *J. Am. Chem. Soc.* **73**, 1431 (1951).
16. A. Ruoff and H. Bürger, *Spectrochim. Acta A* **26**, 989 (1970).
17. R. Anttila, S. Alanko, and V.-M. Horneman, *Mol. Phys.* **102**, 1537 (2008).
18. M. Lewerenz and M. Quack, *Chem. Phys. Lett.* **123**, 197 (1986).
19. S.N. Ghosh, R. Trambarulo, and W. Gordy, *J. Chem. Phys.* **20**, 605 (1952).
20. Y. He, M. Hippler, and M. Quack, *Chem. Phys. Lett.* **289**, 527 (1998).
21. M. Hippler and M. Quack, *Ber. Bunsenges. Phys. Chem.* **99**, 417 (1995).
22. S.N. Delanoye, W.A. Herrebout, and B.J. van der Veken, *J. Am. Chem. Soc.* **124**, 11854 (2002).
23. E.D. Jemmis, K.T. Giju, K. Sundararajan, K. Sankaran, V. Vidya, K.S. Viswanathan, and J. Leszczynski, *J. Mol. Struct.* **510**, 59 (1999).
24. M. Hippler, *J. Chem. Phys.* **127**, 084306 (2007).
25. M. Hippler, *J. Chem. Phys.* **123**, 204311 (2005).
26. A. Trivella, T.N. Wassermann, C. Manca Tanner, N.O.B. Lüttschwager, and S. Coussan, *J. Phys. Chem. A* **122**, 2376 (2018).
27. T.N. Wassermann, D. Luckhaus, S. Coussan, and M.A. Suhm, *Phys. Chem. Chem. Phys.* **8**, 2344 (2006).
28. A. Trivella, T.N. Wassermann, J.M. Mestdagh, C. Manca Tanner, F. Marinelli, P. Roubin, and S. Coussan, *Phys. Chem. Chem. Phys.* **12**, 8300 (2010).
29. T.N. Wassermann, M.A. Suhm, P. Roubin, and S. Coussan, *J. Mol. Struct.* **1025**, 20 (2012).
30. M.A. Suhm and F. Kollipost, *Phys. Chem. Chem. Phys.* **15**, 10702 (2013).
31. C.-C. Yin, A.H.-T. Li, and S.D. Chao, *J. Chem. Phys.* **139**, 194501 (2013).
32. M.J. Frisch, G.W. Trucks, H.B. Schlegel, G.E. Scuseria, M.A. Robb, J.R. Cheeseman, G. Scalmani, V. Barone, B. Mennucci, G.A. Petersson, H. Nakatsuji, M. Caricato, X. Li, H.P. Hratchian, A.F. Izmaylov, J. Bloino, G. Zheng, J.L. Sonnenberg, M. Hada, M. Ehara, K. Toyota, R. Fukuda, J. Hasegawa, M. Ishida, T. Nakajima, Y. Honda, O. Kitao, H. Nakai, T. Vreven, J.A. Montgomery, J.E. Peralta, F. Ogliaro, M. Bearpark, J.J. Heyd, E. Brothers, K.N. Kudin, V.N. Staroverov, R. Kobayashi, J. Normand, K. Raghavachari, A. Rendell, J.C. Burant, S.S. Iyengar, J. Tomasi, M. Cossi, N. Rega, J.M. Millam, M. Klene, J.E. Knox, J.B. Cross, V. Bakken, C. Adamo, J. Jaramillo, R. Gomperts, R.E. Stratmann, O. Yazyev, A.J. Austin, R. Cammi, C. Pomelli, J.W. Ochterski, R.L. Martin, K. Morokuma, V.G. Zakrzewski, G.A. Voth, P. Salvador, J.J. Dannenberg, S. Dapprich, A.D. Daniels, Farkas, J.B. Foresman, J.V. Ortiz, J. Cioslowski, and D.J. Fox, Gaussian Inc. Wallingford CT (2009).
33. J. Bloino and V. Barone, *J. Chem. Phys.* **136**, 124108 (2012).
34. M. Sałdyka, Z. Mielke, K. Mierzwicki, S. Coussan, and P. Roubin, *Phys. Chem. Chem. Phys.* **13**, 13992 (2011).
35. J. Pietilä, S. Alanko, V.-M. Horneman, and R. Anttila, *J. Mol. Spectrosc.* **216**, 271 (2002).
36. S. Coussan, M.E. Alikhani, J.P. Perchard, and W.Q. Zheng, *J. Phys. Chem. A* **104**, 5475 (2000).
37. W. Hujo, M. Gaus, M. Schultze, T. Kubař, J. Grunenberg, M. Elstner, and S. Bauerecker, *J. Phys. Chem. A* **115**, 6218 (2011).
38. S. Oswald, M.A. Suhm, and S. Coussan, *Phys. Chem. Chem. Phys.* **21**, 1277 (2019).
39. E. Mátyus and M.A. Suhm, *Technical report* (2005).

Агрегати хлороформ–азот: підвищення СН та зниження ССІ частот валентних коливань, які спостерігаються в матричній ізоляції та газовому струмені за допомогою інфрачервоної спектроскопії

S. Oswald, S. Coussan

Агрегати хлороформу з азотом вивчені за допомогою широкосмугової інфрачервоної фур'є-спектроскопії в кріогенних матрицях неону, аргону і азоту, а також в надзвукових газових струменях. Валентні коливання СН  $\nu_1$  проявляють «синій» спектральний зсув при переході від газової фази до об'ємних азотних матриць, який можна реконструювати послідовно шляхом поетапного формування кластерів зі збільшенням кількості N<sub>2</sub> як у надзвукових струменях, так і в неонових або аргонових матрицях. Частота валентного коливання ССІ  $\nu_5$ , навпаки, поступово знижується. Невелике підвищення частоти валентного коливання СН спостерігається також і в гомодимері хлороформу.

Ключові слова: надзвуковий газовий струмінь, FTIR, агрегати, частотний зсув.

Агрегаты хлороформ–азот: повышение СН и понижение ССІ частот валентных колебаний, наблюдавшиеся в матричной изоляции и газовой струе с помощью инфракрасной спектроскопии

S. Oswald, S. Coussan

Агрегаты хлороформа с азотом изучены с помощью широкополосной инфракрасной фурье-спектроскопии в криогенных матрицах неона, аргона и азота, а также в сверхзвуковых газовых струях. Валентные колебания СН  $\nu_1$  проявляют «синее» спектральное смещение при переходе от газовой фазы к объемным азотным матрицам, которое можно реконструировать последовательно путем поэтапного формирования кластеров с увеличением количества N<sub>2</sub> как в сверхзвуковых струях, так и в неоновых или аргоновых матрицах. Частота валентного колебания ССІ  $\nu_5$ , наоборот, постепенно понижается. Небольшое повышение частоты валентного колебания СН наблюдается также и в гомодимере хлороформа.

Ключевые слова: сверхзвуковая газовая струя, FTIR, агрегаты, частотный сдвиг.

Supplementary material:  
Chloroform–nitrogen aggregates: upshifted CH and  
downshifted CCl stretching vibrations observed by matrix  
isolation and jet expansion infrared spectroscopy

S. Oswald

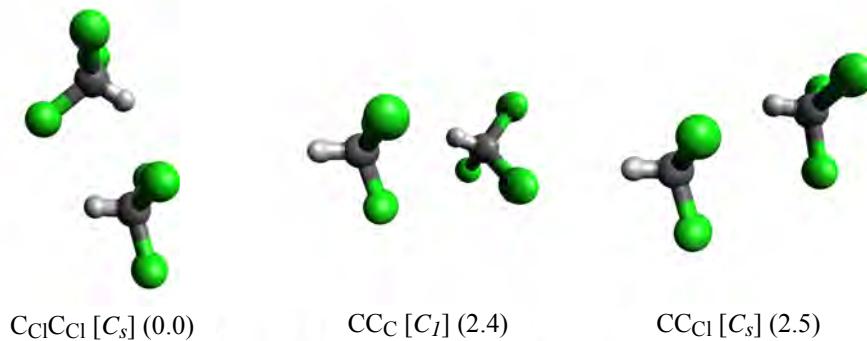
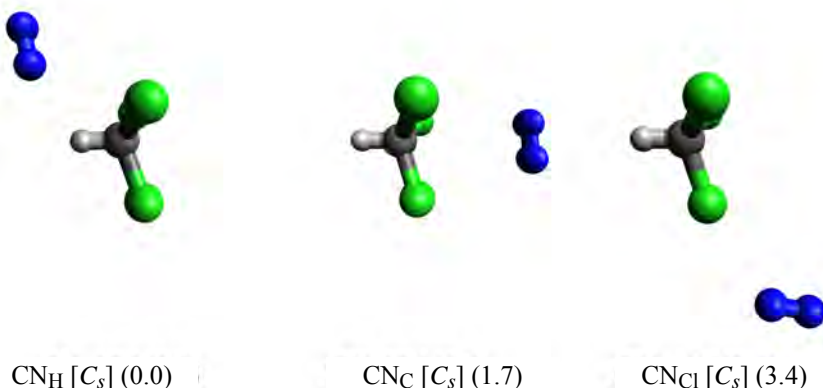
*Institut für Physikalische Chemie, Universität Göttingen, Tammannstr. 6, 37077 Göttingen, Germany*

S. Coussan

*Aix-Marseille Université, CNRS, UMR 7345, Laboratoire Physique des Interactions Ioniques et Moléculaires,  
Marseille, France*  
E-mail: stephane.coussan@univ-amu.fr

Table S1. Gaussian [1] keywords employed in the different calculations

Level of approximation	Employed keywords
B3LYP-D3(BJ)/def2-QZVP	b3lyp, int = superfine, empiricaldispersion = gd3bj, Def2QZVP, fopt = verytight, freq = raman or freq = anharm

Fig. S1. Stable structures of the chloroform dimer optimized at the B3LYP-D3(BJ)/def2-QZVP level. Molecular symmetry point groups are given in brackets, relative energies including harmonic zero-point vibrational energy in  $\text{kJ}\cdot\text{mol}^{-1}$  in parentheses.Fig. S2. Stable structures of the mixed dimer of chloroform and nitrogen optimized at the B3LYP-D3(BJ)/def2-QZVP level of theory. Molecular symmetry point groups are given in brackets, relative energies including harmonic zero-point vibrational energy in  $\text{kJ}\cdot\text{mol}^{-1}$  in parentheses.

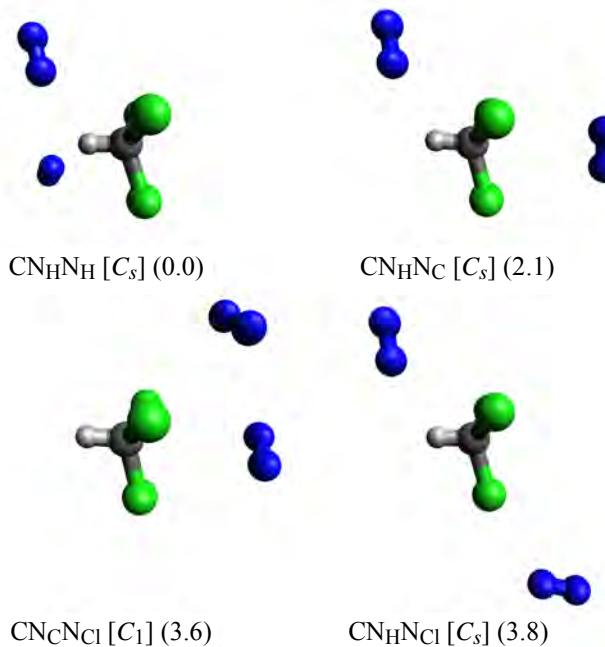


*Fig. S3.* Stable structures of the mixed trimer of chloroform and two nitrogen molecules optimized at the B3LYP-D3(BJ)/def2-QZVP level of theory. Molecular symmetry point groups are given in brackets, relative energies including harmonic zero-point vibrational energy in  $\text{kJ}\cdot\text{mol}^{-1}$  in parentheses.

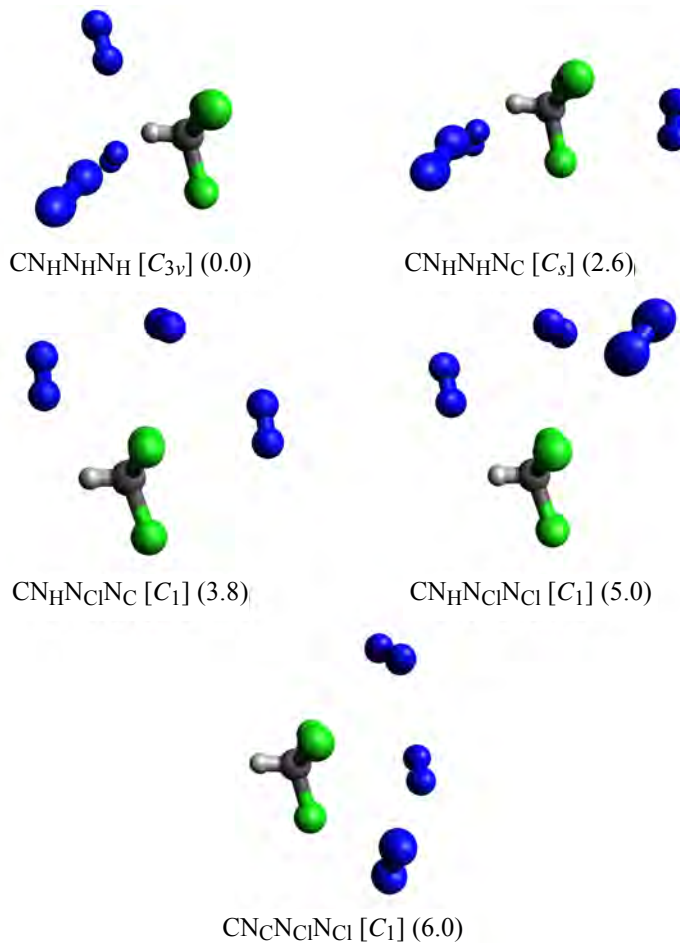


*Fig. S4.* Stable structures of the mixed tetramer of chloroform and three nitrogen molecules optimized at the B3LYP-D3(BJ)/def2-QZVP level of theory. Molecular symmetry point groups are given in brackets, relative energies including harmonic zero-point vibrational energy in  $\text{kJ}\cdot\text{mol}^{-1}$  in parentheses.

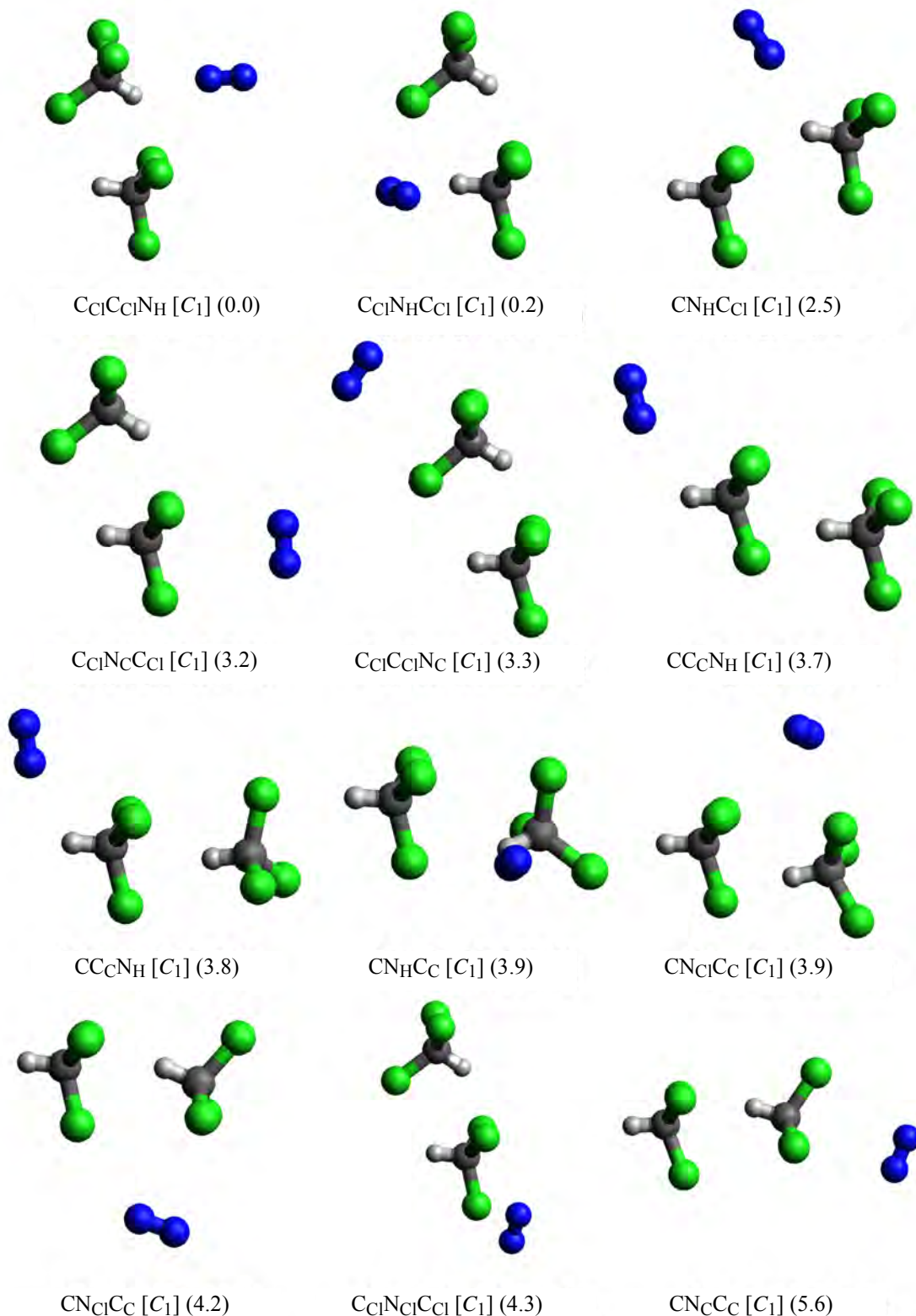


Fig. S5. Stable structures of the mixed trimer of two chloroform and one nitrogen molecules optimized at the B3LYP-D3(BJ)/def2-QZVP level of theory. Molecular symmetry point groups are given in brackets, relative energies including harmonic zero-point vibrational energy in  $\text{kJ}\cdot\text{mol}^{-1}$  in parentheses.

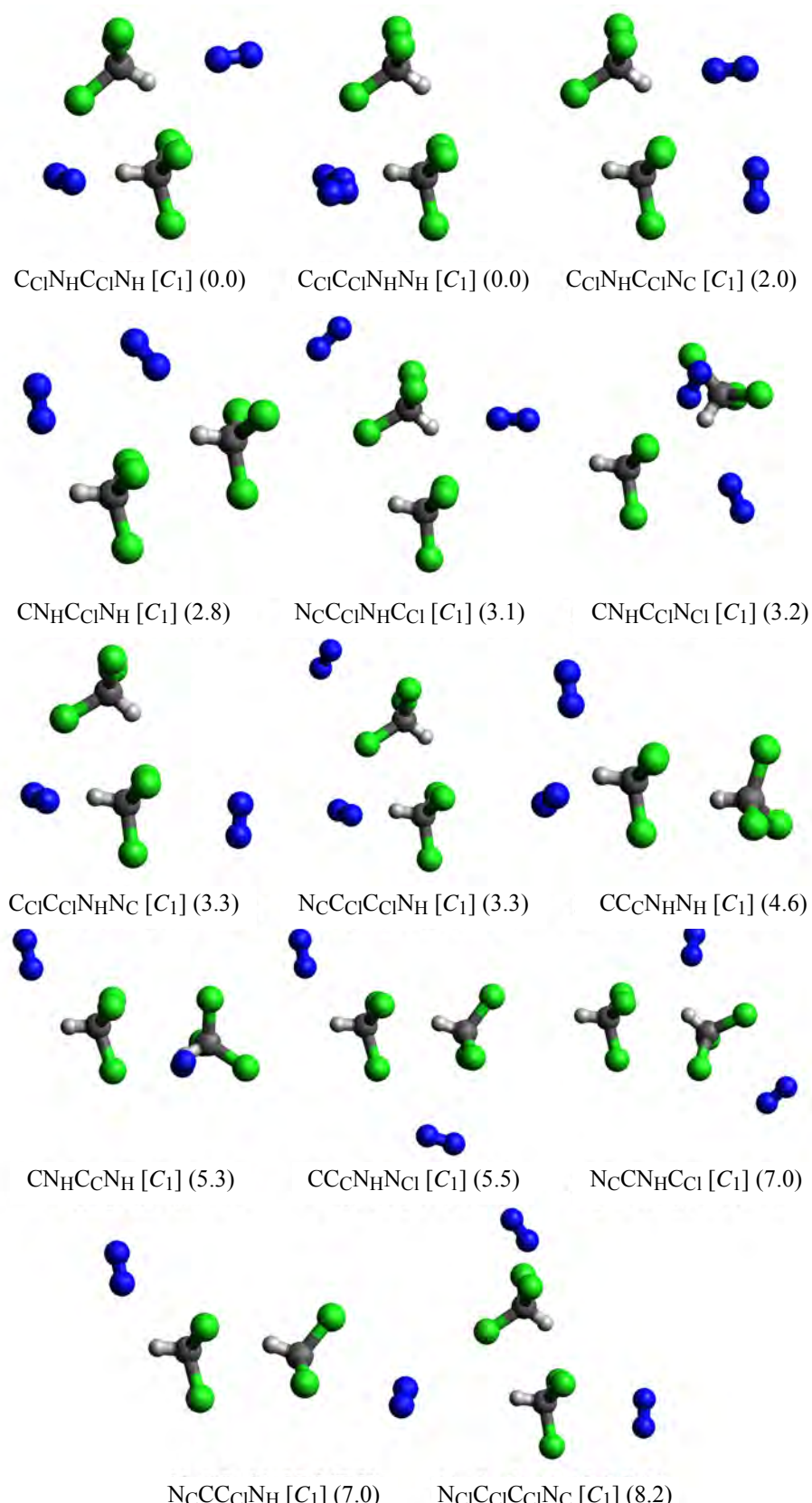


Fig. S6. Stable structures of the mixed tetramer of two chloroform and two nitrogen molecules optimized at the B3LYP-D3(BJ)/def2-QZVP level of theory. Molecular symmetry point groups are given in brackets, relative energies including harmonic zero-point vibrational energy in  $\text{kJ}\cdot\text{mol}^{-1}$  in parentheses.

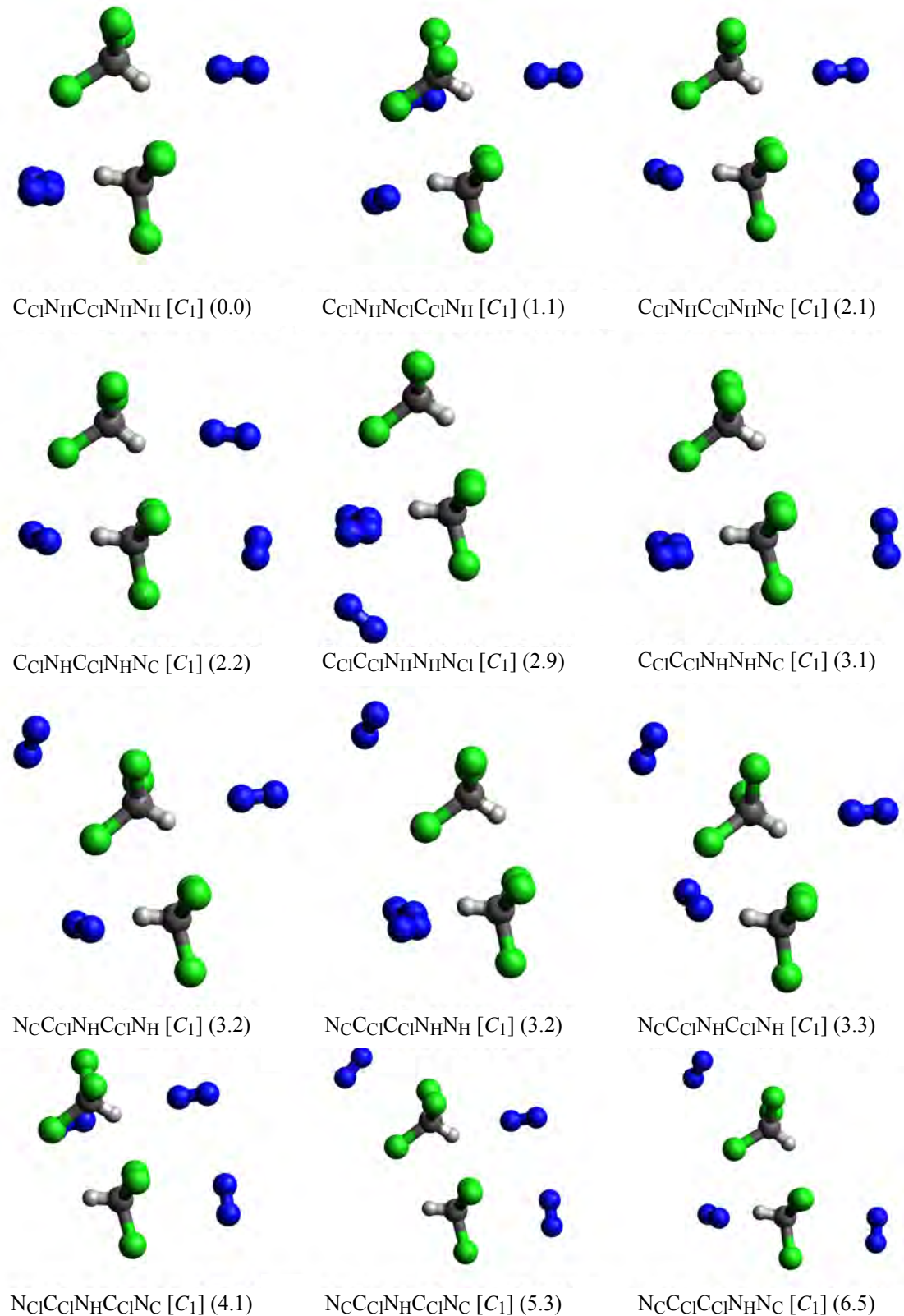


Fig. S7. Stable structures of the mixed pentamer of two chloroform and three nitrogen molecules optimized at the B3LYP-D3(BJ)/def2-QZVP level of theory. Molecular symmetry point groups are given in brackets, relative energies including harmonic zero-point vibrational energy in kJ·mol<sup>-1</sup> in parentheses.

Table S2. Theoretically predicted (for the  $^{35}\text{Cl}$  isotopolog) harmonic ( $\omega_{\text{CH}}$ ) and anharmonic ( $\tilde{\nu}_{\text{CH}}$ ) CH stretching wavenumber in  $\text{cm}^{-1}$ , IR intensity ( $S$ ) in  $\text{km}\cdot\text{mol}^{-1}$ , spectroscopic shifts ( $\Delta\omega_{\text{CH}}$ ,  $\Delta\tilde{\nu}_{\text{CH}}$ ) relative to the corresponding vibration in the pure chloroform monomers or dimers in  $\text{cm}^{-1}$ , lowest predicted harmonic ( $\omega_L$ ) and anharmonic ( $\tilde{\nu}_L$ ) wavenumbers, dissociation energy into the most stable monomers without ( $D_e$ ) and with ( $D_0$ ) harmonic vibrational zero-point energy in  $\text{kJ}\cdot\text{mol}^{-1}$ . All properties were calculated at the B3LYP-D3(BJ)/def2QZVPP level of theory. Anharmonic vibrational frequencies calculated with second order vibrational perturbation theory (Gaussian09 Rev. E01 [1], VPT2 [2]) are unreliable due to unphysical predictions for low-frequency large amplitude motions (indicated by parentheses) which affect localized high-frequency modes like the CH stretching vibration through their respective coupling constants

Structure	$\omega_{\text{CH}}$	$S_\omega$	$\tilde{\nu}_{\text{CH}}$	$S_v$	$\Delta\omega_{\text{CH}}$	$\Delta\tilde{\nu}_{\text{CH}}$	$\omega_L$	$\tilde{\nu}_L$	$D_e$	$D_0$
C	3169	1	3030	0	—	—	258	249	—	—
$\text{C}_{\text{Cl}}\text{C}_{\text{Cl}}$	3183	13	3039	19	14	9	2	(-2876)	17.6	16.0
	3174	5	3034	4	5	4				
$\text{CC}_{\text{C}}$	3185	13	3044	9	16	14	12	(-54)	15.0	13.6
	3170	2	3036	3	1	6				
$\text{CC}_{\text{Cl}}$	3187	12	3047	21	18	17	12	(-35)	14.7	13.5
	3171	2	3041	5	2	11				
$\text{CN}_{\text{H}}$	3185	4	3038	2	16	8	21	(38)	7.2	5.6
$\text{CN}_{\text{C}}$	3170	1	3022	2	1	-8	9	(861)	4.9	3.9
$\text{CN}_{\text{Cl}}$	3169	1	3068	(38)	0	38	4	(517)	3.0	2.2
$\text{CN}_{\text{H}}\text{N}_{\text{H}}$	3199	9	3048	2	30	18	11	(633)	14.8	11.7
$\text{CN}_{\text{H}}\text{N}_{\text{C}}$	3185	5	3052	6	16	22	9	(921)	12.2	9.6
$\text{CN}_{\text{C}}\text{N}_{\text{Cl}}$	3170	1	3041	3	1	11	18	5	10.4	8.1
$\text{CN}_{\text{H}}\text{N}_{\text{Cl}}$	3184	4	3022	3	15	-8	3	3556	10.3	7.9
$\text{CN}_{\text{H}}\text{N}_{\text{H}}\text{N}_{\text{H}}$	3216	17	3078	(726540)	47	48	10	(-3326)	22.8	18.4
$\text{CN}_{\text{H}}\text{N}_{\text{H}}\text{N}_{\text{C}}$	3199	10	3053	12	30	23	8	(-536)	19.8	15.8
$\text{CN}_{\text{H}}\text{N}_{\text{Cl}}\text{N}_{\text{C}}$	3180	3	—	—	11	—	7	—	18.4	14.6
$\text{CN}_{\text{H}}\text{N}_{\text{Cl}}\text{N}_{\text{Cl}}$	3183	4	—	—	14	—	7	—	17.3	13.4
$\text{CN}_{\text{C}}\text{N}_{\text{Cl}}\text{N}_{\text{Cl}}$	3170	1	—	—	1	—	13	—	15.8	12.4
$\text{C}_{\text{Cl}}\text{C}_{\text{Cl}}\text{N}_{\text{H}}$	3201	19	3056	19	18	17	10	(138)	26.6	23.3
	3174	5	3036	5	0	2				
$\text{C}_{\text{Cl}}\text{N}_{\text{H}}\text{C}_{\text{Cl}}$	3189	9	3045	9	6	11	9	(-199)	26.3	23.1
	3180	13	3043	11	6	9				
$\text{CN}_{\text{H}}\text{C}_{\text{Cl}}$	3200	16	3045	11	13	-2	13	(324)	23.8	20.8
	3170	2	3027	3	-1	-14				
$\text{C}_{\text{Cl}}\text{N}_{\text{C}}\text{C}_{\text{Cl}}$	3184	13	3027	2	1	-12	2	(-2490)	22.7	20.1
	3175	5	3043	12	1	9				
$\text{C}_{\text{Cl}}\text{C}_{\text{Cl}}\text{N}_{\text{C}}$	3184	14	3043	17	1	4	3	(-312)	22.6	20.0
	3174	5	3032	5	0	-2				
$\text{CC}_{\text{C}}\text{N}_{\text{H}}$	3186	16	3044	5	1	0	9	(-227)	22.5	19.6
	3185	5	3045	106	15	9				
$\text{CC}_{\text{C}}\text{N}_{\text{H}}$	3187	16	3048	14	2	4	10	(-121)	22.2	19.5
	3186	2	3052	4	1	16				
$\text{CN}_{\text{H}}\text{C}_{\text{C}}$	3185	16	3047	5	0	3	13	(-152)	22.3	19.4
	3170	2	3037	4	0	1				
$\text{CN}_{\text{Cl}}\text{C}_{\text{C}}$	3182	12	3039	5	-3	-5	19	(61)	22.1	19.4
	3170	2	3038	3	0	2				
$\text{CN}_{\text{Cl}}\text{C}_{\text{C}}$	3190	12	3034	20	5	-10	9	(116)	21.5	19.1
	3170	1	3030	0	0	-6				
$\text{C}_{\text{Cl}}\text{N}_{\text{Cl}}\text{C}_{\text{Cl}}$	3183	13	3044	17	0	5	3	(297)	21.4	19.0
	3174	5	3038	6	0	4				
$\text{CN}_{\text{C}}\text{C}_{\text{C}}$	3187	13	3035	7	2	-4	9	(-263)	19.8	17.7
	3171	2	3031	0	1	-5				

$\text{C}_{\text{Cl}}\text{N}_{\text{H}}\text{C}_{\text{Cl}}\text{N}_{\text{H}}$	3199 3189	18 10	— —	— —	16 15	— —	9	—	35.4	30.6
$\text{C}_{\text{Cl}}\text{C}_{\text{Cl}}\text{N}_{\text{H}}\text{N}_{\text{H}}$	3206 3182	16 13	— —	— —	23 8	— —	4	—	35.3	30.6
$\text{C}_{\text{Cl}}\text{N}_{\text{H}}\text{C}_{\text{Cl}}\text{N}_{\text{C}}$	3200 3175	20 5	— —	— —	17 1	— —	10	—	33.1	28.6
$\text{C}\text{N}_{\text{H}}\text{C}_{\text{Cl}}\text{N}_{\text{H}}$	3198 3183	16 5	— —	— —	11 9	— —	12	—	32.5	27.8
$\text{N}_{\text{C}}\text{C}_{\text{Cl}}\text{N}_{\text{H}}\text{C}_{\text{Cl}}$	3201 3175	20 5	— —	— —	18 1	— —	7	—	31.7	27.5
$\text{C}\text{N}_{\text{H}}\text{C}_{\text{Cl}}\text{N}_{\text{Cl}}$	3197 3170	21 1	— —	— —	10 -1	— —	11	—	31.8	27.4
$\text{C}_{\text{Cl}}\text{C}_{\text{Cl}}\text{N}_{\text{H}}\text{N}_{\text{C}}$	3190 3181	10 13	— —	— —	7 7	— —	9	—	31.6	27.3
$\text{N}_{\text{C}}\text{C}_{\text{Cl}}\text{C}_{\text{Cl}}\text{N}_{\text{H}}$	3188 3180	9 13	— —	— —	5 6	— —	7	—	31.5	27.3
$\text{C}\text{C}_{\text{C}}\text{N}_{\text{H}}\text{N}_{\text{H}}$	3201 3189	13 13	— —	— —	16 19	— —	9	—	30.0	26.0
$\text{C}\text{N}_{\text{H}}\text{C}_{\text{C}}\text{N}_{\text{H}}$	3185 3184	2 21	— —	— —	0 14	— —	10	—	29.8	25.3
$\text{C}\text{C}_{\text{C}}\text{N}_{\text{H}}\text{N}_{\text{Cl}}$	3192 3186	14 4	— —	— —	7 16	— —	7	—	29.0	25.1
$\text{N}_{\text{C}}\text{C}\text{N}_{\text{H}}\text{C}_{\text{Cl}}$	3186 3170	17 2	— —	— —	-1 -1	— —	10	—	27.5	23.6
$\text{N}_{\text{C}}\text{C}\text{C}_{\text{Cl}}\text{N}_{\text{H}}$	3189 3186	17 4	— —	— —	2 15	— —	8	—	27.3	23.6
$\text{N}_{\text{C}}\text{I}\text{C}_{\text{Cl}}\text{C}_{\text{Cl}}\text{N}_{\text{C}}$	3182 3175	13 5	— —	— —	-1 1	— —	1	—	25.8	22.4
$\text{C}_{\text{Cl}}\text{N}_{\text{H}}\text{C}_{\text{Cl}}\text{N}_{\text{H}}\text{N}_{\text{H}}$	3206 3200	17 18	— —	— —	23 26	— —	7	—	44.4	38.0
$\text{C}_{\text{Cl}}\text{N}_{\text{H}}\text{N}_{\text{Cl}}\text{C}_{\text{Cl}}\text{N}_{\text{H}}$	3198 3189	18 10	— —	— —	15 15	— —	11	—	43.1	36.9
$\text{C}_{\text{Cl}}\text{N}_{\text{H}}\text{C}_{\text{Cl}}\text{N}_{\text{H}}\text{N}_{\text{C}}$	3198 3190	19 10	— —	— —	15 16	— —	10	—	42.0	35.9
$\text{C}_{\text{Cl}}\text{N}_{\text{H}}\text{C}_{\text{Cl}}\text{N}_{\text{H}}\text{N}_{\text{C}}$	3201 3190	19 9	— —	— —	18 16	— —	10	—	41.9	35.8
$\text{C}_{\text{Cl}}\text{C}_{\text{Cl}}\text{N}_{\text{H}}\text{N}_{\text{H}}\text{N}_{\text{Cl}}$	3206 3182	15 13	— —	— —	23 8	— —	4	—	41.0	35.1
$\text{C}_{\text{Cl}}\text{C}_{\text{Cl}}\text{N}_{\text{H}}\text{N}_{\text{H}}\text{N}_{\text{C}}$	3207 3183	17 14	— —	— —	24 9	— —	4	—	40.6	34.9
$\text{N}_{\text{C}}\text{C}_{\text{Cl}}\text{N}_{\text{H}}\text{C}_{\text{Cl}}\text{N}_{\text{H}}$	3198 3189	19 10	— —	— —	15 15	— —	8	—	40.7	34.8
$\text{N}_{\text{C}}\text{C}_{\text{Cl}}\text{C}_{\text{Cl}}\text{N}_{\text{H}}\text{N}_{\text{H}}$	3206 3182	16 14	— —	— —	23 8	— —	6	—	40.4	34.8
$\text{N}_{\text{C}}\text{C}_{\text{Cl}}\text{N}_{\text{H}}\text{C}_{\text{Cl}}\text{N}_{\text{H}}$	3194 3182	18 10	— —	— —	11 8	— —	8	—	40.7	34.7
$\text{N}_{\text{C}}\text{I}\text{C}_{\text{Cl}}\text{N}_{\text{H}}\text{C}_{\text{Cl}}\text{N}_{\text{C}}$	3197 3174	19 4	— —	— —	14 0	— —	8	—	39.6	33.9
$\text{N}_{\text{C}}\text{C}_{\text{Cl}}\text{N}_{\text{H}}\text{C}_{\text{Cl}}\text{N}_{\text{C}}$	3200 3175	21 5	— —	— —	17 1	— —	7	—	38.2	32.8
$\text{N}_{\text{C}}\text{C}_{\text{Cl}}\text{C}_{\text{Cl}}\text{N}_{\text{H}}\text{N}_{\text{C}}$	3189 3181	10 13	— —	— —	6 7	— —	7	—	36.7	31.5

Table S3. Theoretically predicted (for the  $^{35}\text{Cl}$  isotopolog) harmonic ( $\omega_{\text{CCl}}$ ) and anharmonic ( $\tilde{\nu}_{\text{CCl}}$ ) CCl stretching wavenumber in  $\text{cm}^{-1}$ , IR intensity ( $S$ ) in  $\text{km}\cdot\text{mol}^{-1}$ , spectroscopic shift ( $\Delta\omega_{\text{CCl}}$ ) relative to the corresponding vibration in the pure chloroform monomers or dimers in  $\text{cm}^{-1}$ , lowest predicted harmonic ( $\omega_L$ ) and anharmonic ( $\tilde{\nu}_L$ ) wavenumbers, dissociation energy into the most stable monomers without ( $D_e$ ) and with ( $D_0$ ) harmonic vibrational zero-point energy in  $\text{kJ}\cdot\text{mol}^{-1}$ . All properties were calculated at the B3LYP-D3(BJ)/def2QZVP level of theory. Anharmonic vibrational frequencies calculated with second order vibrational perturbation theory (Gaussian09 Rev. E01 [1], VPT2 [2]) are unreliable due to unphysical predictions for low-frequency large amplitude motions which affect localized high-frequency modes like the CH stretching vibration through their respective coupling constants

Structure	$\omega_{\text{CCl}}$	$S_\omega$	$\tilde{\nu}_{\text{CCl}}$	$S_\nu$	$\Delta\omega_{\text{CCl}}$	$\omega_L$	$\tilde{\nu}_L$	$D_e$	$D_0$
C	733	161	699	161	–	258	249	–	–
	733	161	727	168	–				
$\text{C}_{\text{Cl}}\text{C}_{\text{Cl}}$	744	228	725	203	11				
	742	123	735	25	9				
	725	220	706	195	–8	2	(–2876)	17.6	16.0
	723	38	701	53	–10				
$\text{CC}_\text{C}$	740	260	722	254	7				
	737	261	718	279	4				
	734	28	716	28	1	12	(–54)	15.0	13.6
	722	16	702	28	–11				
$\text{CC}_{\text{Cl}}$	738	243	719	214	5				
	738	263	721	218	5				
	729	15	712	44	–4	12	(–35)	14.7	13.5
	723	23	704	28	–10				
$\text{CN}_\text{H}$	736	169	716	165	3				
	732	153	714	151	–1	21	(38)	7.2	5.6
$\text{CN}_\text{C}$	733	150	720	165	0				
	732	155	716	170	–1	9	(861)	4.9	3.9
$\text{CN}_{\text{Cl}}$	735	166	706	110	2				
	732	161	709	104	–1	4	(517)	3.0	2.2
$\text{CN}_{\text{H}}\text{N}_{\text{H}}$	737	167	714	147	4				
	732	155	713	159	–1	11	(633)	14.8	11.7
$\text{CN}_{\text{H}}\text{N}_{\text{C}}$	736	158	716	133	3				
	731	147	710	128	–2	9	(921)	12.2	9.6
$\text{CN}_{\text{C}}\text{N}_{\text{Cl}}$	733	151	712	137	0				
	732	146	711	133	–1	18	5	10.4	8.1
$\text{CN}_{\text{H}}\text{N}_{\text{Cl}}$	738	174	725	202	5				
	731	153	719	179	–2	3	(3556)	10.3	7.9
$\text{CN}_{\text{H}}\text{N}_{\text{H}}\text{N}_{\text{H}}$	735	160	2487	(59829)	2				
	735	160	(–1058)	(25455)	2	10	(–3326)	22.8	18.4
$\text{CN}_{\text{H}}\text{N}_{\text{H}}\text{N}_{\text{C}}$	736	160	716	131	3				
	732	144	716	128	–1	8	(–536)	19.8	15.8
$\text{CN}_{\text{H}}\text{N}_{\text{Cl}}\text{N}_{\text{C}}$	737	170	–	–	4				
	730	133	–	–	–3	7	–	18.4	14.6
$\text{CN}_{\text{H}}\text{N}_{\text{Cl}}\text{N}_{\text{Cl}}$	737	178	–	–	4				
	732	142	–	–	–1	7	–	17.3	13.4
$\text{CN}_{\text{C}}\text{N}_{\text{Cl}}\text{N}_{\text{Cl}}$	733	149	–	–	0				
	732	139	–	–	–1	13	–	15.8	12.4
$\text{C}_{\text{Cl}}\text{C}_{\text{Cl}}\text{N}_{\text{H}}$	744	193	727	212	0				
	741	151	724	120	–1				
	727	208	710	184	2	10	(138)	26.6	23.3
	723	53	705	59	0				

$\text{C}_{\text{Cl}}\text{N}_{\text{H}}\text{C}_{\text{Cl}}$	744	207	728	281	0	9	(-199)	26.3	23.1
	742	142	726	112	0				
	726	205	710	183	1				
	723	54	708	50	0				
$\text{C}\text{N}_{\text{H}}\text{C}_{\text{Cl}}$	741	292	723	401	3	13	(324)	23.8	20.8
	737	178	723	648	-1				
	734	81	716	88	5				
	722	14	707	56	-1				
$\text{C}_{\text{Cl}}\text{N}_{\text{C}}\text{C}_{\text{Cl}}$	744	221	729	198	0	2	(-2490)	22.7	20.1
	742	113	734	45	0				
	725	217	707	288	0				
	722	38	704	63	-1				
$\text{C}_{\text{Cl}}\text{C}_{\text{Cl}}\text{N}_{\text{C}}$	743	211	725	567	-1	3	(-312)	22.6	20.0
	742	139	731	508	0				
	725	204	707	216	0				
	722	39	705	123	-1				
$\text{CC}_{\text{C}}\text{N}_{\text{H}}$	741	263	721	452	1	9	(-227)	22.5	19.6
	737	261	717	200	0				
	734	27	716	265	0				
	723	15	688	610	1				
$\text{CC}_{\text{C}}\text{N}_{\text{H}}$	739	261	721	255	-1	10	(-121)	22.2	19.5
	738	251	723	235	1				
	729	12	712	16	-5				
	724	19	707	27	2				
$\text{C}\text{N}_{\text{H}}\text{C}_{\text{C}}$	742	247	724	258	2	13	(-152)	22.3	19.4
	735	171	718	143	-2				
	731	110	714	103	-3				
	723	33	707	48	1				
$\text{C}\text{N}_{\text{Cl}}\text{C}_{\text{C}}$	740	241	725	231	0	19	(61)	22.1	19.4
	737	272	718	257	0				
	734	24	717	30	0				
	722	14	704	35	0				
$\text{C}\text{N}_{\text{Cl}}\text{C}_{\text{C}}$	740	264	728	601	0	9	(116)	21.5	19.1
	737	233	727	234	0				
	730	19	719	577	-4				
	722	27	704	194	0				
$\text{C}_{\text{Cl}}\text{N}_{\text{Cl}}\text{C}_{\text{Cl}}$	744	222	700	377	0	3	(297)	21.4	19.0
	742	122	731	93	0				
	725	207	713	207	0				
	723	49	698	48	0				
$\text{C}\text{N}_{\text{C}}\text{C}_{\text{C}}$	738	252	722	379	-2	9	(-263)	19.8	17.7
	738	238	724	278	-1				
	729	15	713	142	-5				
	722	21	705	25	-1				
$\text{C}_{\text{Cl}}\text{N}_{\text{H}}\text{C}_{\text{Cl}}\text{N}_{\text{H}}$	743	180	-	-	-1	9	-	35.4	30.6
	741	160	-	-	-1				
	727	215	-	-	2				
	723	51	-	-	0				
$\text{C}_{\text{Cl}}\text{C}_{\text{Cl}}\text{N}_{\text{H}}\text{N}_{\text{H}}$	744	222	-	-	0	4	-	35.3	30.6
	742	127	-	-	0				
	726	211	-	-	1				
	724	51	-	-	1				

$\text{CClN}_\text{H}\text{CClN}_\text{C}$	743	191	–	–	–1	10	–	33.1	28.6
	741	133	–	–	–1				
	727	211	–	–	2				
	722	50	–	–	–1				
$\text{CN}_\text{H}\text{CClN}_\text{H}$	742	272	–	–	4	12	–	32.5	27.8
	737	131	–	–	–1				
	735	142	–	–	6				
	721	17	–	–	–2				
$\text{N}_\text{C}\text{CClN}_\text{H}\text{CCl}$	743	172	–	–	–1	7	–	31.7	27.5
	741	170	–	–	–1				
	726	198	–	–	1				
	722	48	–	–	–1				
$\text{CN}_\text{H}\text{CClN}_\text{Cl}$	740	260	–	–	2	11	–	31.8	27.4
	737	194	–	–	–1				
	732	107	–	–	3				
	725	10	–	–	2				
$\text{CClC}_\text{ClN}_\text{H}\text{N}_\text{C}$	744	208	–	–	0	9	–	31.6	27.3
	742	124	–	–	0				
	726	208	–	–	1				
	722	51	–	–	–1				
$\text{N}_\text{C}\text{CClC}_\text{ClN}_\text{H}$	743	159	–	–	–1	7	–	31.5	27.3
	742	186	–	–	0				
	726	185	–	–	1				
	722	63	–	–	–1				
$\text{CC}_\text{C}\text{N}_\text{H}\text{N}_\text{H}$	740	257	–	–	0	9	–	30.0	26.0
	738	235	–	–	1				
	730	23	–	–	–4				
	722	24	–	–	0				
$\text{CN}_\text{H}\text{C}_\text{C}\text{N}_\text{H}$	741	247	–	–	1	10	–	29.8	25.3
	735	201	–	–	–2				
	730	94	–	–	–4				
	725	20	–	–	3				
$\text{CC}_\text{C}\text{N}_\text{H}\text{N}_\text{Cl}$	742	260	–	–	2	7	–	29.0	25.1
	737	221	–	–	0				
	731	29	–	–	–3				
	721	31	–	–	–1				
$\text{N}_\text{C}\text{CN}_\text{H}\text{CCl}$	742	237	–	–	4	10	–	27.5	23.6
	734	165	–	–	–4				
	731	111	–	–	2				
	723	31	–	–	0				
$\text{N}_\text{C}\text{CClN}_\text{H}$	740	248	–	–	2	8	–	27.3	23.6
	738	221	–	–	0				
	729	28	–	–	0				
	721	28	–	–	–2				
$\text{N}_\text{Cl}\text{CClC}_\text{ClN}_\text{C}$	745	221	–	–	1	1	–	25.8	22.4
	742	114	–	–	0				
	725	211	–	–	0				
	722	51	–	–	–1				
$\text{CClN}_\text{H}\text{CClN}_\text{H}\text{N}_\text{H}$	744	191	–	–	0	7	–	44.4	38.0
	741	149	–	–	–1				
	728	210	–	–	3				
	724	57	–	–	1				

$\text{C}_\text{Cl}\text{N}_\text{H}\text{N}_\text{Cl}\text{C}_\text{Cl}\text{N}_\text{H}$	744	186	–	–	0	11	–	43.1	36.9
	740	176	–	–	-2				
	728	161	–	–	3				
	723	84	–	–	0				
$\text{C}_\text{Cl}\text{N}_\text{H}\text{C}_\text{Cl}\text{N}_\text{H}\text{N}_\text{C}$	743	187	–	–	-1	10	–	42.0	35.9
	741	132	–	–	-1				
	727	220	–	–	2				
	723	47	–	–	0				
$\text{C}_\text{Cl}\text{N}_\text{H}\text{C}_\text{Cl}\text{N}_\text{H}\text{N}_\text{C}$	743	201	–	–	-1	10	–	41.9	35.8
	740	118	–	–	-2				
	727	219	–	–	2				
	723	46	–	–	0				
$\text{C}_\text{Cl}\text{C}_\text{Cl}\text{N}_\text{H}\text{N}_\text{H}\text{N}_\text{Cl}$	744	222	–	–	0	4	–	41.0	35.1
	742	128	–	–	0				
	726	202	–	–	1				
	724	62	–	–	1				
$\text{C}_\text{Cl}\text{C}_\text{Cl}\text{N}_\text{H}\text{N}_\text{H}\text{N}_\text{C}$	744	221	–	–	0	4	–	40.6	34.9
	742	110	–	–	0				
	726	217	–	–	1				
	723	44	–	–	0				
$\text{N}_\text{C}\text{C}_\text{Cl}\text{N}_\text{H}\text{C}_\text{Cl}\text{N}_\text{H}$	743	139	–	–	-1	8	–	40.7	34.8
	741	197	–	–	-1				
	728	199	–	–	3				
	723	54	–	–	0				
$\text{N}_\text{C}\text{C}_\text{Cl}\text{C}_\text{Cl}\text{N}_\text{H}\text{N}_\text{H}$	744	177	–	–	0	6	–	40.4	34.8
	742	169	–	–	0				
	727	176	–	–	2				
	723	73	–	–	0				
$\text{N}_\text{C}\text{C}_\text{Cl}\text{N}_\text{H}\text{C}_\text{Cl}\text{N}_\text{H}$	742	94	–	–	-2	8	–	40.7	34.7
	740	241	–	–	-2				
	730	205	–	–	5				
	720	39	–	–	7				
$\text{N}_\text{Cl}\text{C}_\text{Cl}\text{N}_\text{H}\text{C}_\text{Cl}\text{N}_\text{C}$	743	177	–	–	-1	8	–	39.6	33.9
	740	163	–	–	-2				
	727	182	–	–	2				
	722	64	–	–	-1				
$\text{N}_\text{C}\text{C}_\text{Cl}\text{N}_\text{H}\text{C}_\text{Cl}\text{N}_\text{C}$	743	174	–	–	-1	7	–	38.2	32.8
	741	148	–	–	-1				
	726	202	–	–	1				
	722	45	–	–	-1				
$\text{N}_\text{C}\text{C}_\text{Cl}\text{C}_\text{Cl}\text{N}_\text{H}\text{N}_\text{C}$	743	168	–	–	-1	7	–	36.7	31.5
	742	158	–	–	0				
	726	190	–	–	1				
	722	57	–	–	1				

Table S4. Cartesian coordinates (in Å) of computed N monomer from B3LYP-D3(BJ)/def2-QZVP geometry optimizations in Gaussian 09 Revision E.01

	N		
N	0.00000	0.00000	0.54501
N	0.00000	0.00000	-0.54501

Table S5. Cartesian coordinates (in Å) of computed C monomer from B3LYP-D3(BJ)/def2-QZVP geometry optimizations in Gaussian 09 Revision E.01

	C		
C	0.00000	0.00000	0.45599
H	0.00000	0.00000	1.53580
Cl	0.00000	1.69095	-0.08376
Cl	1.46441	-0.84548	-0.08376
Cl	-1.46441	-0.84548	-0.08376

Table S6. Cartesian coordinates (in Å) of computed  $\text{CCl}|\text{CCl}$  dimer from B3LYP-D3(BJ)/def2-QZVP geometry optimizations in Gaussian 09 Revision E.01

	$\text{CCl} \text{CCl}$		
C	0.15303	-1.83706	0.00000
H	0.72972	-0.92501	0.00000
C	-0.30861	2.01195	0.00000
H	-1.25998	1.50121	0.00000
Cl	0.56621	-2.74355	1.46487
Cl	-1.56925	-1.37873	0.00000
Cl	0.56621	-2.74355	-1.46487
Cl	-0.60950	3.75602	0.00000
Cl	0.56621	1.50710	1.46337
Cl	0.56621	1.50710	-1.46337

Table S7. Cartesian coordinates (in Å) of computed  $\text{CC}_\text{C}$  dimer from B3LYP-D3(BJ)/def2-QZVP geometry optimizations in Gaussian 09 Revision E.01

	$\text{CC}_\text{C}$		
C	0.75980	-1.35010	0.00000
H	0.63797	-0.27825	0.00000
C	-1.01811	2.21608	0.00000
H	-1.48418	3.19014	0.00000
Cl	-0.01619	-1.98274	1.46400
Cl	-0.01619	-1.98274	-1.46400
Cl	2.50334	-1.68705	0.00000
Cl	-2.29764	0.99075	0.00000
Cl	-0.01619	2.09243	1.46286
Cl	-0.01619	2.09243	-1.46286

Table S8. Cartesian coordinates (in Å) of computed  $\text{CC}_{\text{Cl}}$  dimer from B3LYP-D3(BJ)/def2-QZVP geometry optimizations in Gaussian 09 Revision E.01

	$\text{CC}_{\text{Cl}}$		
C	1.70387	-0.03300	-0.01498
H	0.86777	-0.10024	-0.69344
C	-2.44288	0.04016	-0.50998
H	-3.34994	0.12101	-1.09017
Cl	-2.89453	-0.10231	1.19522
Cl	-1.57734	-1.40973	-1.07133
Cl	-1.48225	1.50596	-0.80420
Cl	1.07464	-0.23436	1.63028
Cl	2.84267	-1.32989	-0.43138
Cl	2.44364	1.56659	-0.22839

Table S9. Cartesian coordinates (in Å) of computed  $\text{CN}_{\text{H}}$  dimer from B3LYP-D3(BJ)/def2-QZVP geometry optimizations in Gaussian 09 Revision E.01

	$\text{CN}_{\text{H}}$		
C	-0.13365	0.53722	0.00000
H	0.94539	0.53156	0.00000
Cl	-0.67396	2.22717	0.00000
Cl	-0.67396	-0.31008	1.46372
Cl	-0.67396	-0.31008	-1.46372
N	2.34704	-1.68365	0.00000
N	2.54273	-2.75551	0.00000

Table S10. Cartesian coordinates (in Å) of computed  $\text{CN}_{\text{H}}\text{N}_{\text{H}}$  trimer from B3LYP-D3(BJ)/def2-QZVP geometry optimizations in Gaussian 09 Revision E.01

	$\text{CN}_{\text{H}}\text{N}_{\text{H}}$		
C	0.03615	-0.73988	0.00000
H	0.70836	0.10324	0.00000
Cl	0.35317	-1.68984	-1.46490
Cl	-1.62060	-0.09922	0.00000
Cl	0.35317	-1.68984	1.46490
N	0.69092	1.95905	1.83149
N	0.35317	2.57504	2.66437
N	0.69092	1.95905	-1.83149
N	0.35317	2.57504	-2.66437

Table S11. Cartesian coordinates (in Å) of computed  $\text{CN}_\text{H}\text{N}_\text{H}\text{N}_\text{H}$  tetramer from B3LYP-D3(BJ)/def2-QZVP geometry optimizations in Gaussian 09 Revision E.01

	$\text{CN}_\text{H}\text{N}_\text{H}\text{N}_\text{H}$		
C	0.00000	0.00000	0.88588
H	0.00000	0.00000	-0.19147
Cl	0.00000	1.69079	1.42660
Cl	1.46427	-0.84540	1.42660
Cl	-1.46427	-0.84540	1.42660
N	0.00000	-2.12177	-1.66275
N	0.00000	-3.14181	-2.04586
N	1.83751	1.06089	-1.66275
N	2.72089	1.57090	-2.04586
N	-1.83751	1.06089	-1.66275
N	-2.72089	1.57090	-2.04586

Table S12. Cartesian coordinates (in Å) of computed  $\text{C}_\text{Cl}\text{C}_\text{Cl}\text{N}_\text{H}$  trimer from B3LYP-D3(BJ)/def2-QZVP geometry optimizations in Gaussian 09 Revision E.01

	$\text{C}_\text{Cl}\text{C}_\text{Cl}\text{N}_\text{H}$		
C	-1.75368	-0.47759	-0.00687
H	-0.93616	0.20910	-0.15648
C	2.12415	-0.44509	-0.00361
H	1.71996	-1.44555	0.03697
Cl	-2.87928	-0.28065	-1.36063
Cl	-1.07825	-2.12669	0.02488
Cl	-2.52139	-0.07736	1.53852
Cl	3.89054	-0.55270	0.03454
Cl	1.55584	0.29587	-1.51739
Cl	1.49919	0.43868	1.40565
N	-0.87845	2.74623	-0.18836
N	-0.68435	3.81390	-0.09053

Table S13. Cartesian coordinates (in Å) of computed  $\text{C}_\text{Cl}\text{N}_\text{H}\text{C}_\text{Cl}\text{N}_\text{H}$  tetramer from B3LYP-D3(BJ)/def2-QZVP geometry optimizations in Gaussian 09 Revision E.01

	$\text{C}_\text{Cl}\text{N}_\text{H}\text{C}_\text{Cl}\text{N}_\text{H}$		
C	-1.84718	0.52687	-0.25037
H	-1.24168	-0.35631	-0.12427
C	1.89898	-0.51310	-0.35646
H	1.74523	0.47433	-0.76342
Cl	-2.34964	1.07362	1.35841
Cl	-0.84576	1.75925	-1.05799
Cl	-3.24216	0.08828	-1.25046
Cl	3.63249	-0.86712	-0.39939
Cl	1.28496	-0.49942	1.31162
Cl	0.97981	-1.65962	-1.35792
N	2.32167	3.53917	1.07774
N	2.33142	2.74164	0.33547
N	-1.73434	-3.48805	1.60218
N	-1.72297	-2.56639	1.02119

Table S14. Cartesian coordinates (in Å) of computed  $\text{C}_{\text{Cl}}\text{N}_\text{H}\text{C}_{\text{Cl}}\text{N}_\text{H}\text{N}_\text{H}$  pentamer from B3LYP-D3(BJ)/def2-QZVP geometry optimizations in Gaussian 09 Revision E.01

	$\text{C}_{\text{Cl}}\text{N}_\text{H}\text{C}_{\text{Cl}}\text{N}_\text{H}\text{N}_\text{H}$		
C	1.91689	-0.77844	-0.04704
H	1.47961	0.19776	-0.18204
C	-1.57151	0.93891	-0.01571
H	-1.66390	-0.13497	0.00596
Cl	2.74548	-0.78880	1.51894
Cl	0.59532	-1.97223	-0.07675
Cl	3.04917	-1.05268	-1.38197
Cl	-3.19900	1.63172	0.03599
Cl	-0.61622	1.42577	1.40176
Cl	-0.73316	1.37537	-1.52285
N	-2.36568	-2.14871	2.92987
N	-2.35598	-1.63396	1.96961
N	2.77378	3.56429	-0.05515
N	2.51058	2.51268	-0.16467
N	-2.57008	-1.69621	-1.80772
N	-2.73476	-2.24822	-2.73256

- M.J. Frisch, G.W. Trucks, H.B. Schlegel, G.E. Scuseria, M.A. Robb, J.R. Cheeseman, G. Scalmani, V. Barone, B. Mennucci, G.A. Petersson, H. Nakatsuji, M. Caricato, X. Li, H.P. Hratchian, A.F. Izmaylov, J. Bloino, G. Zheng, J.L. Sonnenberg, M. Hada, M. Ehara, K. Toyota, R. Fukuda, J. Hasegawa, M. Ishida, T. Nakajima, Y. Honda, O. Kitao, H. Nakai, T. Vreven, J.A. Montgomery, J.E. Peralta, F. Ogliaro, M. Bearpark, J.J. Heyd, E. Brothers, K.N. Kudin, V.N. Staroverov, R. Kobayashi, J. Normand, K. Ragahavachari, A. Rendell, J.C. Burant, S.S. Iyengar, J. Tomasi, M. Cossi, N. Rega, J.M. Millam, M. Klene, J.E. Knox, J.B. Cross, V. Bakken, C. Adamo, J. Jaramillo, R. Gomperts, R.E. Stratmann, O. Yazyev, A.J. Austin, R. Cammi, C. Pomelli, J.W. Ochterski, R.L. Martin, K. Morokuma, V.G. Zakrzewski, G.A. Voth, P. Salvador, J.J. Dannenberg, S. Dapprich, A.D. Daniels, Ö. Farkas, J.B. Foresman, J.V. Ortiz, J. Cioslowski, and D.J. Fox, Gaussian 09 Revision E.01, Gaussian Inc. Wallingford CT (2009).
- J. Bloino and V. Barone, *J. Chem. Phys.* **136**, 124108 (2012).